THE UNIVERSITY OF MICHIGAN

INDUSTRY PROGRAM OF THE COLLEGE OF ENGINEERING

A STUDY OF BORON IN CAST AUSTENITIC IRON-BASE HEAT-RESISTANT ALLOYS

R. Wayne Kraft, Jr.

A dissertation submitted in partial fulfillment
of the requirements for the degree of
Doctor of Philosophy in the
University of Michigan
1958

June, 1958

IP-302

PREFACE

I wish to express my appreciation to all those who have aided in this investigation and particularly to the following:

My wife, for her continuous encouragement, unselfishness, understanding, and patience.

Professor Richard A. Flinn, Chairman of my Doctoral Committee, for his continued interest, patient guidance, and helpful suggestions during this investigation.

Professor James A. Freeman, member of the Doctoral Committee, for his friendly advice and helpful comments.

Professors W. C. Bigelow, C. C. Craig, E. E. Hucke, and L. Thomassen, members of the Doctoral Committee, for their interest and cooperation.

Chrysler Corporation for sponsorship of much of this work and financial assistance.

My fellow graduate students in Metallurgical Engineering for their cooperation, assistance, and enlightening discussions.

Messrs. J. Cuneo, N. Hozak, J. Hoffman, J. VanderSluis, and Miss Christine Sadler for their assistance in the experimental phases of this program.

The Industry Program of the College of Engineering for the production of this thesis.

TABLE OF CONTENTS

TABLE OF CONTENTS (concluded)

LIST OF TABLES

LIST OF FIGURES

LIST OF FIGURES (concluded)

LIST OF APPENDICES

INTRODUCTION

A few years prior to World War II, boron was added to ferrous alloys intentionally, on a commercial basis, for the first time for the purpose of promoting hardenability.[1] During the war such steels became more widely used because of the savings realized in strategic alloy content. Since that time, the element has also been found to enhance the high-temperature properties of a number of the so-called high-temperature super alloys, and even more recently it has been found that it prevents strain-aging in low-carbon open-hearth steels.[2] As with many metallurgical developments, the effects were established prior to the causes. For example, even now there is not complete agreement on the mechanism by which a minute amount of boron has such a pronounced effect upon the hardenability of steel.

This dissertation is concerned, not with the hardenability effect, but rather with the role of boron in high-temperature heat-resistant alloys. More specifically, it was found during the early stages of a recently completed alloy development program that boron caused a progressive increase in the 10- and 100-hr rupture strengths of a cast iron-base austenite (18% Ni and 18% Cr) at 1500°F—even up to the 1.5% boron level.[3] Since this is far more boron than is usually added to high-temperature alloys—by orders of magnitude—it was decided to study this phenomenon by attempting to delineate the probable mechanism by which such large amounts of boron enhance the high-temperature properties of cast iron-base austenites.

REVIEW OF LITERATURE

The pertinent literature on the subject can be classified for convenience into three categories: 1) mechanical property data, 2) physical behavior, and 3) phase equilibria and identification of compounds.

Literature Pertaining to Mechanical Properties of Boron Alloys

One of the earliest investigators who studied alloys of this type, Wasmuht,[4] added boron in amounts up to 1.14% to a series of steels, some of which were 18% Cr—8% Ni austenites. He observed that the austenitic steels showed a pronounced increase in hardness upon tempering at 1292-1472°F (700-800°C) after having been quenched from a high temperature. Since the microstructures showed a characteristic precipitate phase throughout the matrix as a result of this treatment, he deduced that the observed behavior was a precipitation-hardening phenomenon. Bennek and Schafmeister[5] also found that alloys of this type were precipitation-hardenable. Their investigations were concerned primarily with the corrosion resistance of two phase alloys for cutlery applications. They noted, as had their predecessor, that large amounts of boron caused the formation of a second phase (prior to precipitation-hardening) which embrittled the alloy.

It was not until several years later that Cornelius,[6] while studying the effects of boron in a series of austenites with varying chromium, nichel, and carbon contents, noted that precipitation-hardening would not occur at low carbon contents. He found that a minimum of .07% C was necessary to produce any precipitation-hardening. Both Wasmuht's and

Bennek and Schafmeister's alloys contained appreciable amounts of carbon (.15%). Cornelius also reported that the high-temperature heat treatment (2192°F-1200°C) spheroidized the boride phase (which he assumed to be primarily iron borides) and that tempering—today it is called aging heat treatment—did not cause any further change in the microstructure or hardness of the low-carbon alloys. The high-carbon alloys, on the other hand, were quite susceptible to solution-treating and subsequent aging in the temperature range of 932-1652°F (500-900°C).

Wasmuht was the only one of these early German investigators who performed any elevated temperature tests and his results are limited to hot tensile tests for one alloy for testing temperatures up to 1242°F (700°C). Chronologically speaking, Comstock[7] was the first who emphasized that boron would enhance the high-temperature properties of wrought steels. He showed that it was necessary to deoxidize the steel with aluminum prior to the boron addition, and that niobium or titanium was needed to stabilize carbon to achieve the maximum effects from boron present in amounts from .01 to .10% by weight. Miller, Smith, and Porter[8] found that boron (and niobium) improve the high-temperature strength of 18-8 stainless steels. These results were derived from short-time rupture tests (100-hr maximum) at temperatures of 1200, 1400, and 1600°F (649, 760, and 871°C). Guy[9] obtained similar results. All these investigators were reporting experimental facts. Apparently none of them studied in detail the mechanism by which boron increased the high-temperature properties.

Additional work with boron was done by Corey and Freeman,[10] who examined the effects of boron and boron plus titanium on a 13% Cr—15% Ni—2% Mo—.6% W wrought high-temperature alloy. The maximum boron content investigated was 0.23%. Hardness surveys, microstructures, lattice-parameter measurements, and 100-hr rupture strengths at 1200°F (649°C)

were used to evaluate the response of the materials to various processing treatments. It was found that boron was more effective in promoting the 1200°F (649°C) rupture strength when titanium was also present. With 0.6% titanium, for example, a maximum in the curves of rupture strength versus percent boron was observed at 0.09% B for both the solution-treated and hot—cold-worked samples. In the absence of titanium, increasing boron (up to 0.23% B) caused a progressive rise in the rupture strength, but the highest values observed were still lower than the maxima of the Ti-B curves. Corey and Freeman concluded that precipitation-hardening was not the major factor and that solid solution-strengthing by the boron was appreciable. It appeared that a reaction analogous to strain-aging was promoted by hot-cold work. Possible alternative mechanisms suggested by the authors were that boron might render an unknown detrimental alloying element or phase inactive through formation of inert secondary phases; or that boron increased the resistance to recovery from cold work or strain-hardening during testing.

All the work which has been reviewed thus far was done on wrought alloys. Other investigators, however, have found similar beneficial effects attributable to boron in cast alloys. Blatz, Reynolds, and Dyrkacz[11] observed that 1% B increased the 100-hr and 1000-hr rupture strengths at 1500 to 1800°F (816 to 982°C) of S816 alloy (0.4% C, 1.2% Mn, 0.4% Si, 20% Cr, 20% Ni, 4% Mo, 4% W, 4% Nb and Ta, balance Co). The alloys had good ductility as measured in the rupture tests. More boron than 1.0% caused a decrease in the rupture strength. Strauss,[12] in discussing the above paper, said that he had obtained similar results during the war on complex W-Cr-Ni-Co alloys. In this case the optimum boron content varied from 0.5 to 2.5% B, and he suggested that future work might well be done with higher amounts of boron, the remainder of the analysis being balanced

to suit, rather than turning toward smaller boron percentages. None of these authors described any detailed studies which would indicate how such large amounts of boron were effective in increasing hot strength.

Contrasted to the work on these high boron alloys is that done by several men on alloys containing much smaller quantities of boron. Koffler, Pennington, and Richmond[13] found that boron (and zirconium), within the percentages studied, .01% maximum, definitely improved the rupture life and ductility of vacuum-melted nickel-base and cobalt-base alloys tested in either the wrought or as-cast condition. The amount of improvement varied from grade to grade. This improvement in properties was not obtained at the expense of increased first-stage creep or increased minimum creep rate. Confirmation of these results was obtained by Decker, Rowe, and Freeman.[14] These researchers also found that the small, but important, amount of boron and/or zirconium which produced such outstanding results was often inadvertently introduced into the melt by crucible contamination. Quite recently, another paper by Pennington[15] has appeared. The beneficial effects of small amounts of boron (and zirconium) are reported for several vacuum-melted nickel- and cobalt-base alloys—M252, J1570, Nimonic 90, Waspalloy, and A286. Decker[16] studied the mechanism of the beneficial effects of trace amounts of boron and zirconium and concluded that very small quantities of the elements under discussion increased the properties of a complex Ti and Al hardened nickel-base alloy by retarding structural changes at the grain boundaries. Boron and zirconium delayed microcracking during creep rupture testing until the later stages. It was postulated that the most likely reason for this retardation effect was that boron and zirconium segregated preferentially at the grain boundaries.

Literature Pertaining to Physical Behavior of Boron in Austenite

It is a simple geometrical fact that the boron atom is too large to dissolve interstitially to any great extent in face-centered cubic iron or nickel. It is also too small to dissolve substitutionally in appreciable quantities, since the difference in atomic diameter between nickel or iron and boron is greater than 15%. Since the question of the location of the boron atoms in austenite is of paramount importance in understanding the mechanism by which a small quantity of boron can have a very profound effect on the hardenability of constructional steels, this phase of the problem has been studied quite intensively. Inasmuch as this dissertation is also concerned with boron in austenite, it seemed appropriate to review the literature from this viewpoint.

There seems to be no question that boron is very probably concentrated at the grain boundaries.[17,18,19] This configuration will be the most stable,[20] although it is unlikely that a continuous film of boron per se is present at the grain boundaries.[21] Stated another way, it has been shown that the boron undergoes positive adsorption to gamma grain boundaries and that the temperature coefficient of adsorption is positive,[22] which means that the boron will tend to segregate in increasing amounts with increasing temperature. In addition to undergoing this type of adsorption, which has been termed equilibrium segregation, boron also dissolves to a limited extent in γ iron and to a lesser extent in α iron. The phase relations are reviewed in the next section, but it should be mentioned here that probably boron dissolves substitutionally in α iron and interstitially in γ iron. Some conflicting evidence has been obtained, however.[22]

Literature Pertaining to Phase Equilibria and Identification of Boride Compounds

In preliminary experiments of this study, it was noted that as the

boron content of Fe-Ni-Cr alloys was increased, an increasing amount of a hard phase (presumably a boride or borides) occurred. This of course is nothing new. Almost all the authors mentioned previously have observed this phenomenon, but none of them has unequivocably identified the phases except in the simplest Fe-B alloys. For this reason a systematic search was made for all pertinent phase diagrams and x-ray diffraction data of boride phases.

Iron-Boron System

Equilibrium Diagram.—Wever and Muller[23] published the first reliable iron-boron diagram. The very low boron region of the diagram has since been redetermined by others.[24,25] Intermetallic compounds corresponding to Fe_2B and FeB are formed. A eutectic occurs between Fe_2B and γ at about 2100-2130°F (1149-1165°C) and at 3.8% B. The maximum solubility of B in γ is 0.021% at this temperature. The solubility of B in γ decreases to about 0.002 to 0.001% by weight at 1663-1672°F (906-911°C), at which temperature the transformation to the α phase involves a peritectoid reaction. The details of the diagram are in doubt here, but it is certain that the solubility of B in α iron is very low at lower temperatures (0.0004% at 1310°F or 710°C).

X-ray Diffraction Data.—Fe_2B is tetragonal and FeB is orthorhombic. The space lattices have been determined and the diffraction patterns published.[26,27,28]

Chromium-Boron System

Equilibrium Diagram.—No phase diagram has been published of this alloy system. The solubility of boron in the chromium lattice is "very low."[29] Several boride phases which correspond approximately to the formulae Cr_2B, Cr_3B_2, CrB, Cr_3B_4, and CrB_2 have been reported.[30]

X-ray Diffraction.—The maximum boron content of any of the alloys studied in this investigation or which have been reported in the literature is less than 15 atomic percent boron and usually much less than this amount. For this reason the borides of lowest boron content are of most interest.

Anderson and Kiessling[31] determined that the Cr_2B phase is orthorhombic. They reported the lattice constants but did not report any diffraction data from which the phase could be identified. Through the courtesy of Dr. R. Steinitz,[32] a sample of Cr_2B was procured from which the diffraction data were obtained. Cr_2B is apparently a unique diboride since it is not isomorphous with other borides of the type Me_2B.[29] Anderson and Kiessling gave diffraction data on the CrB phase.

Nickel-Boron System

Equilibrium Diagram.—Four boride phases were identified in this alloy system when it was first reported.[33] Typically, the solubility of boron in nickel is very low, although the exact value has not been accurately determined. A series of eutectic points occurs between the borides, the first at the low boron side of the diagram at 4.0% B and 2084°F (1140°C) between nickel and Ni_2B. More recently, a lower boride, Ni_3B, has been reported,[31,34] making the series, listed in order of increasing boron content, Ni_3B, Ni_2B, Ni_3B_2, NiB, Ni_2B_3 (or NiB_2). The compositions expressed by these formulae are extremely doubtful, however.[32]

X-ray Diffraction Data.—Diffraction data from which orthorhombic Ni_3B can be identified have been published by Rundqvist.[34] Similar information for the tetragonal Ni_2B compound was presented by others.[26,31,35]

Ternary Systems

The only pertinent ternary involving boron which has been investigated is the Cr-Ni-B system. Post, Pipitz, and Herz[36] reported the existence of an orthorhombic phase with a very narrow composition range which corresponds to the formula Cr_2NiB_4. They believed that this phase is an ordered modification of Cr_3B_4. X-ray diffraction data were given.

Summary of Literature Review

Boron, although it dissolves to only a very limited extent in most alloys, has a very pronounced effect upon the high-temperature properties. Trace amounts of boron apparently segregate to the grain boundaries of wrought alloys where they delay microcracking and hence increase the strength. When the boron content of wrought alloys is increased by another order of magnitude (0.05-0.20% range), additional mechanisms such as strain-aging or solid solution-strengthening (or perhaps others) appear to be responsible for the increase in strength. At still higher boron contents (0.5-2.0% range), a beneficial effect has been observed in a variety of alloys but the mechanism is not understood. Alloys in this category are usually used in the as-cast condition because of the presence of a large amount of excess boride phase which embrittles the material.

It was decided, therefore, to study a group of relatively simple alloys containing large amounts of boron (and which exhibited the beneficial effects) with the objective of establishing the role of boron in cast alloys.

EXPERIMENTAL PROCEDURES

The general procedure followed in this work was to make a series of investment-cast test-bar heats by vacuum induction melting. The principal variable in the heats was boron content which varied from 0 to 1.49% B. After a careful inspection, and in some cases after a pretreatment (heat treatment and/or prestressing at room temperature), the creep and rupture properties of the heats were evaluated at 1500°F (816°C). Supplementary laboratory investigations, such as metallographic inspection, microhardness measurements, x-ray diffraction analyses, chemical analyses, and so forth, were performed to study the mechanisms involved. A detailed description of the various processes follows.

The descriptions are given in the sequence in which the data were obtained, namely, molding, melting, inspection, rupture testing (sometimes preceded by heat treating), and metallographic examination. This section is concluded with a description of the x-ray diffraction techniques, chemical analysis methods, and diffusion experiment techniques.

Investment Molding

A photograph of a pattern cluster of wax tensile bar patterns is shown in Fig. 1. The actual tensile specimen was one with a nominal .250-in. diameter by 1-in. gage length. The pins projecting from the shoulders of the specimens were produced as an integral part of the castings to facilitate subsequent attachment of the extensometers used in creep testing. Each bar was individually risered, as shown, to insure radiographic soundness.

These clusters were dipcoated and invested with a refractory slurry

of the ethyl silicate type.[37] After hardening, the molds were dewaxed at a temperature of about 300°F (149°C). They were then fired at a temperature of 1800°F (982°C) preparatory to pouring. [For those few heats which were poured to evaluate the rupture properties of argon-melted material, the firing temperature was 1600°F (871°C).]

Melting Procedures

With the exception of a few heats which were poured to compare the rupture properties of argon versus vacuum atmospheres in melting, all the experimental work was done on vacuum-melted material.

Vacuum-Melting

Vacuum-melting was performed in the apparatus shown in Fig. 2. Prior to actual melting, a stabilized zirconia crucible was rammed into place within the induction core and outgassed by heating a steel ingot placed within the crucible to a temperature in excess of 2000°F (1093°C). (Care was taken not to melt the ingot.) This was done at a reduced pressure. In fact, the ingot was kept hot until all the gases (primarily water vapor from the ramming mix) were evolved. This could be determined by noting when the pressure had stabilized over a period of at least 15 min at a pressure of less than 10μ of mercury.

The charge materials were electrolytic nickel squares and shot, electrolytic chromium, either electrolytic iron or armco iron (see Tables I and II), nickel boron as a source of boron, and aluminum for deoxidizing as 2S aluminum wire. The chromium was always placed within the crucible with as much of the nickel and iron as possible since it was found that if the chromium were added to a molten both of iron and nickel, severe gas evolution (probably hydrogen) would splash metal out of the crucible. After the chromium and a portion of the nickel and iron melted, the bal-

ance of the nickel and iron was added by means of the charging buckets shown in Fig. 3. The heat weight was 2600 gm.

At this point in the melting procedure, the heat was kept molten but not allowed to exceed approximately 2900°F (1593°C) by alternately applying and interrupting the power until the pressure gages indicated stabilization at a value less than 5μ. Then 0.10% Al was added to insure effective deoxidation of the melt,[1,38] and shortly thereafter the nickel boron was added.

Temperatures were measured on the earlier heats (lower heat numbers) with a platinum—10% rhodium platinum thermocouple encased in a fused silica tube. Later on, a long sighting tube was added to the vacuum equipment and a Leeds and Northrup optical pyrometer was used.

As soon as all the alloys were added, the power was cut off and the heat allowed to freeze. Immediately thereafter the vacuum pumps were closed and argon gas was admitted to the tank. This was necessary to lift the cover so that the hot investment mold could be placed into pouring position. Then the cover was closed again and the argon gas pumped out. When the Stokes manometer gage showed that the pressure within the tank had been reduced to the neighborhood of from 1000 to 2000μ, the power was again applied. Ordinarily this process took no longer than a few minutes and the pressure was 25μ by the time the heat had remelted. The purpose of admitting argon rather than air was to minimize the chance of contaminating the heat (even though it was not molten) with nitrogen or oxygen, from the air while the investment mold was being placed into position. During the remelting interval, the power was increased to the maximum and usually the melt reached the pouring temperature of 2850°F (1566°C) within 14 to 15 min from the time that the cover had been opened to admit the mold. Thermocouple surveys had shown that

the mold cavity would have cooled to about 1500°F (816°C) from 1800°F (982°C) during this 15-min interval. As soon as the pouring temperature was reached, the heat was poured. The molds were kept in the vacuum chamber until the castings had solidified.

Argon-Melting

Zirconia crucibles were used with a small induction furnace similar to that shown in Fig. 3. During the course of meltdown, a cover brick was placed on top of the furnace and argon gas was continuously admitted through an opening above the liquid metal level in the crucible. Actual pouring was accomplished by clamping the hot investment mold to the top of the furnace and rotating the entire assembly. As soon as the mold-furnace assembly had been rotated, the argon-gas flow was increased until a line pressure of at least 5 psi was observed. This pressure was then above the liquid metal and provided extra metallostatic pressure. This technique of pressure pouring improved the quality of the castings. The molds for argon-melted heats were fired at 1600°F (871°C) rather than 1800°F (982°C) because the time lag between removal of mold from the firing furnace and pouring was only 2 to 3 min as compared to 14 to 15 min for the vacuum heats. A narrow range of pouring temperatures was developed in this manner.

Inspection

The investment cast molds were allowed to cool in air for a period of at least 4 hr before shakeout. After a light sand blast, the test bars were removed from the gating system by an abrasive cutoff wheel and uniquely identified with a vibratory pencil.

To supplement the visual inspection made after cleaning, the tensile bars from each heat were radiographed. Only those bars which exhibited

no radiographic indications of internal defects and which passed the visual examination for surface defects were used for tensile or stress-rupture testing. The unacceptable tensile bars were used for metallographic purposes, chemical analysis, etc.

Stress-Rupture Testing

Stress-rupture and creep testing was done in resistance-wire heated testing units. Strain was transmitted, by means of extensometers attached to the pins on the test specimens, to an optical lever system with a sensitivity of 0.000005 in./in. The specimens were inserted into the testing furnace about 15 hr prior to application of the load. During the first 12 hr the specimens were brought to a temperature of about 1400°F (760°C) and the temperature over the gage length was equalized (as determined by three chromel-alumel thermocouples spanning the gage length) to within less than ±3.0°F (±1.7°C). When thermal equilibrium was reached, the furnace temperature was raised to 1500°F (816°C) and checked again for gradients. After the temperature had equalized over the gage length at this test temperature, the load was applied and the deformation during loading was recorded.

Heat-Treating

Several types of heat-treating experiments were performed. The method which was used depended on the material being heat-treated and the temperature of treatment.

High-temperature heat treatment of large solid samples such as test bars was conducted in a Surface Combustion Corp. gas-fired furnace into which a closed-end magnesite tube (2-1/4-in. ID) had been installed as a muffle. The closed end of the tube was placed near the center of the furnace. The tube projected through a hole in the door of the furnace so

that the open or cold end of the tube was outside the furnace. This end was equipped with an asbestos board plug through which two holes had been made. One hole served as an inlet port for the argon gas which was metered through the tube throughout the heat treatment at a rate of 1 ℓ/min minimum. A chromel-alumel thermocouple strung with porcelain insulators was admitted through the other hole. This plug was packed with asbestos paper after the charge was in place. Temperature control was achieved by means of the thermocouple placed within the tube, at the end of the tube adjacent to the specimen. The couple was connected to a Brown Electronik high-speed recorder. Normal temperature variation did not exceed ± 5°F (2.8°C) at heat-treating temperatures of 2150°F (1177°C) during a 24-hr run.

For convenience, small metallographic samples were sometimes heat-treated in a Leco tube type furnace tyrough which argon gas was admitted. Temperature control again was achieved by means of a thermocouple placed next to the specimen within the tube.

Powdered samples (filings) were sealed into short sections of fused silica tubing under vacuum (approximately 1-mm Hg). The samples were heat-treated in a Hayes electric globar type furnace; the control couple again was placed on top of the sample.

The lower-temperature heat treatments [1700°F (927°C) or less] were done in small Hoskins resistance furnaces. In general, no provision was made to provide an inert atmosphere since the oxidation of the samples at these lower temperatures was not apparent. Filings, however, were sealed in quartz tubing, even at these temperatures.

Metallography

Polishing and Etching Technique

Microspecimens were prepared in the conventional manner and polished manually with successively finer papers. Further polishing was done on polishing wheels, first with 6-micron diamond and then with Linde B abrasive. Final polishing and etching was done electrolytically with a solution consisting of 10% perchloric acid, 90% glacial acetic acid. The current density varied considerably with the specimen being treated, and had to be determined experimentally. Samples for optical microscopic examination and photomicrography were polished for 3 sec. It was found that the samples for microhardness measurements should be electrolytically polished for at least 30 sec (with the current on and off for ten 3-sec intervals to prevent overheating of the solution) if reliable readings were to be obtained. Apparently, the metal was deeply enough cold-worked during polishing through the papers that 30 sec of electrolytic polishing was required to get beneath the cold-worked layer. Actually, a 60-sec etch was used to insure that the microhardness readings would be representative of the specimen. This severe etching procedure caused the borides to stand out in such bold relief that samples so etched were not suitable for photomicrography.

Microhardness Measurements

The hardness of the austenite and/or boride phase in these alloys was measured with a Reichert microhardness accessory for a Reichert Wien optical microscope. For all the data reported on the austenitic phase, a load of 18.3 gm was used. This irrational load was much more reproducible and convenient, because of the design of the hardness accessory, than a more conventional load of perhaps 10, 15, or 20 gm. For the harder

boride phases, a 50-gm load was used so that the size of the impression produced was large enough to be accurately measured.

At least 25 hardness impressions were made in all cases. The diagonal lengths of these impressions were measured with the special eyepiece supplied with the microscope. The mean, standard deviation, and 95% confidence limits for the mean were calculated according to standard statismethods.[39] The average hardness and 95% confidence limits for the hardness were then computed. A sample calculation is shown in Appendix I.

An attempt was made to distinguish between the hardness of the center of austenite grains and the hardness of the austenite adjacent to boride particles. Since absolutely no difference between these two zones could be observed statistically, no distinction was made as to where the hardness impressions were taken. Occasionally, however, an abnormally hard reading was observed. This could always be detected and was caused by the presence of a hard boride particle just below the surface of the sample. Such a reading was discarded and other measurements were taken. Similarly, but less frequently, abnormally low readings were noticed. These, caused by microshrinkage immediately below the surface, were also discarded.

Point-Counting

Measurements of the volume percentage of boride phase in the microstructures were obtained by placing a standard grain-size measuring eyepiece on the microscope. The eyepiece had two sets of five parallel lines each intersecting at right angles. The 25 points of intersection were the points which were counted as either boride or austenite. In practice, a magnification was chosen so that the structure appeared coarse enough to permit easy interpretation. The number of intersection points superim-

posed over boride and over austenite was noted. Then the stage of the microscope was moved so that a new field of view was under observation and another count was taken. This was repeated 200 times for each specimen, so that in all 5000 points were counted. The data are summarized in Table III.

X-Ray Diffraction

Two types of procedures require description—the method used in determining the lattice constant of the austenite and that used to identify the borides.

Lattice-Parameter Measurements of Austenite

Two different methods of specimen preparation and two methods of determining the lattice constant were used.

Specimen Preparation.—Several attempts were made to determine the lattice constant of the austenite on solid samples—metallographic specimens, for example. However, because of the coarse grain structure of these alloys, satisfactory photographs could not be produced, even with oscillation and rotation of the specimen in the cameras during exposure. It was therefore necessary to prepare filings of the materials.

In the first method of specimen preparation, filings were obtained (always using a clean file for each sample) from the solid sample under study after its surface had been ground clean. These filings were then sealed in fused silica tubes under reduced pressure and brought to a temperature of 1300°F (704°C) for a period not exceeding 15 min. The annealing treatment was necessary since it was found that the cold-work introduced by the filing operation was sufficient to cause such severe line broadening that the resulting x-ray diffraction photographs were worthless for the intended purpose.

An alternate method of sample preparation was used to evaluate the effect of the 1300°F (704°C) treatment on the lattice parameter. It could only be done for the samples which were heat-treated. This method consisted of preparing the filings and then subjecting the filings which had been sealed in quartz to the high-temperature heat treatment. The lattice parameter was measured after 2150°F (1177°C) treatment and then again after an additional 1300°F (704°C) heat treatment.

X-Ray Methods.—The two methods used to determine the lattice constant (of the filings) were the back-reflection method and the powder method. All measurements were made at ambient temperature [72 ± 5°F (22.2± 2.8°C)].

The back-reflection method is generally considered to be superior to the powder method for the precision determination of lattice constants because of the greater resolving power obtained in a back-reflection focusing camera and because the systematic errors inherent in x-ray diffraction approach zero at the higher Bragg angles.[40] For these reasons the back-reflection method employing unfiltered chromium radiation was used. The specimens were prepared on cardboard holders according to a method described by Byrne and Hansen.[41] After 6-hr exposures, the films were processed according to the procedure recommended by the manufacturers.

The lattice constant was computed from the measurements of the diffraction lines for each of the three lines ($220\alpha_1$, $220\alpha_2$, 311β) on desk computing machines. At least seven figures were carried throughout to avoid the introduction of computational errors. These values were plotted versus $\cos^2\theta$ and the extrapolated value (to $\cos^2\theta = 0$) was used as the best value of the lattice constant. Even though this extrapolation technique compensates for film shrinkage during processing, the measured θ values of the diffraction lines were corrected for film shrinkage prior to computation of the lattice constant. This was done by measuring the knife-

edge marks which also appeared on the film and which corresponded to θ values of 85°, 80°, 75°, ..., 60°. Using these nominal θ values, and the calculated values for the knife-edge marks, a correction curve was obtained for each film, from which film-shrinkage corrections for the diffraction lines were obtained. Some typical extrapolation curves of lattice constant versus $\cos^2\theta$ are shown at the left side of Fig. 4.

Even though the back-reflection method is theoretically superior to the powder method for precision determination of lattice constants (for a camera of the same diameter), as pointed out before, in these particular alloys the back-reflection method is disadvantageous since only three diffraction lines are observed, and two of these form a doublet and are therefore very close together. A glance at the left side of Fig. 4 will show that the extrapolated value of the lattice constant is completely dependent upon the values calculated from the 220 and 311 reflections. If one of these measurements is seriously in error, then the extrapolated value is in error. Furthermore, since the extrapolation curve is really just drawn between two points (the doublet lines being very close together), there is no way of detecting errors.

Because of these limitations, the powder method was also used with large cameras (114.6-mm diam) and unfiltered chromium radiation. Special care was taken with sample preparation and alignment to insure that the sharpest possible diffraction lines would be produced. Five-hour exposures were found adequate. After these the film was processed as described. Lattice-parameter computations were made according to the method of Nelson and Riley[42] after the films had previously been corrected for film shrinkage. A few typical results are shown on the right side of Fig. 4 for the same samples on which back-reflection data were obtained.

The chief advantage for this investigation of the powder

technique as compared to the back-reflection method is that, if a significant error has occurred in the measurement or calculation for one of the high-angle lines, it becomes readily apparent; several points are used to establish the curve rather than just three as in the back-reflection method. For this reason, the powder method as described was used for the bulk of the lattice-constant determinations in this report.

Boride Identification

Very early in this investigation, it was determined that some method must be devised to separate the boride (the minor phase) from the austenite to study more effectively the nature of this precipitate.

Extraction and Sample Preparation.—A bromine extraction method developed by Mahla and Nielsen[43] was used for most of the work. A small sample of the material to be investigated was cleaned (by sanding or grinding) to remove any thick surface oxide or other phase resulting from a mold-metal interaction. It was then immersed in a solution of 10% bromine in anhydrous methyl alcohol and allowed to digest for a period of time, the length of which depended on how much precipitate was needed and how much was present in the alloy. It was determined that the bromine solution did dissolve the boride phase, but at a very much lower rate than was observed for the austenite phase. For the samples in question, an extraction period from 30 to 60 min was used. At the end of this time, the sample tubes were centrifuged for 4 min. The remainder of the solid sample and the bromine solution were then removed; the samples were washed and rewashed with methyl alcohol and centrifuged 4 min each time until all visible traces of the bromine had disappeared.

[To obtain enough of this residue for wet chemical analysis, an anodic

disintegration technique was necessary before the bromine treatment. More specifically, it was found that the time required to dissolve 1 or 2 cc of solid metal (which was the amount required to produce a sufficient volume of precipitate) took over 48 hr and that in this length of time a significant amount of the precipitate also dissolved. Therefore a sample of the solid metal was made the anodic member of a simple electrolytic cell. A 3- to 4-hr run at a current of about 2 amp and 6 v in a 10% HCl electrolyte yielded a comparatively large amount of residue at the bottom of the cell. This residue was not pure boride (austenite diffraction lives could still be observed and the austenite could be seen in a microspecimen which was prepared), so it was subjected to the bromine treatment for 1 hr to remove the remaining austenite.]

X-Ray Methods.—X-ray diffraction photographs were made of all the residues extracted in the manner outlined above. A smaller Debye-Scherer camera (57.3-mm diam) was used to reduce exposure times. Filtered chromium radiation was employed. Theta values were corrected for film shrinkage according to the method of Straumanis,[40] and from these values the d spacings were determined from plots of Bragg's law.

Chemical Analysis

Samples from the gage lengths of the five original heats were analyzed for Ni, Cr, B, C, N, and O, and also analyzed spectroscopically. Boron, of course, was the primary variable studied for this report. Its analysis was the most difficult—and the most expensive ($30 - $35 per determination)—so that for the other heats, where actual boron analyses could not be determined and where it was desired to evaluate the effect of heat treatment (or some other variable) on stress-rupture properties, at least one stress-rupture bar was always reserved for testing in the as-cast condition. In this way an indirect comparison with the five original heats was possible

because they were tested in the as-cast condition.

Nickel, Chromium, and Carbon

The analyses for these elements (and also iron) were performed by one laboratory. The techniques were conventional wet chemical methods (combustion for carbon), so the details need not be given here.

Boron

Boron analyses were run on samples from heats R308 through R312 by two different commercial laboratories and one industrial laboratory. These have been designated Laboratories A, B, and C (not necessarily listed respectively).

Laboratory A determined the boron content by treating the samples with HCl under refluxing conditions. The residue was filtered off and fused with alkaline flux such as sodium carbonate plus sodium nitrate or sodium peroxide. This material was put into solution and the boron determined on the combined solutions by the usual distillation techniques in an anhydrous system.

Laboratory B used a procedure devised by Wolszon, Hayes, and Hill.[44] It was quite similar to the method followed by Laboratory A. One of the differences was that hydrogen peroxide was added to the hydrochloric acid solution to facilitate dissolving by refluxing of the samples. Fusion with an alkaline flux of a portion of the residue was therefore unnecessary.

Laboratory C dissolved the sample of about 2 gm by refluxing in 20 ml of 6N HCl until the solution was complete (2 to 4 hr). Sufficient sodium hydroxide was then added to neutralize 9 cc of the hydrochloric acid. From this point on the procedure was as described by L. V. Wilcox.[45]

Oxygen and Nitrogen

Chemical analyses for these gaseous elements were performed on the National Research Corp. vacuum fusion apparatus at The University of Michigan.

Diffusion Experiments

Samples for diffusion studies were machined to dimensions of .450-in. diam by .450-in. height from the ring gate (see Fig. 1) of the 0% boron heat, R310. A 1/16-in. (.0625 in.) diam hole was drilled to within 1/32 in. of one base through the center of each sample. Elemental boron was packed into these cavities which were then plugged with a short section of 1/16-in.-diam 18-8 stainless-steel weld rod. The final step in the preparation of the sample consisted of fusing the stainless-steel plug to the sample by means of an oxy-acetylene welding torch, thus completely sealing the boron within the austenitic iron slug.

The actual diffusion was carried out in the Leco furnace under an atmosphere of argon. One sample was run for 24 hr at 2300°F (1260°C), and the other for 1-1/2 hr at 2150°F (1177°C). Following this thermal treatment, the slugs were sectioned through the center on a jeweler's cutoff wheel and mounted for metallographic examination.

RESULTS

In this section the actual results of the experimental work are presented for three types of specimens: as-cast, heat-treated, and pre-stressed and heat-treated. Each of these sections is further subdivided for convenience.

After all the data have been given, they are discussed and appropriate conclusions are drawn in the next section.

As-Cast Material

Heats R308 through R312 are a series which contain approximately 18.5% Ni, 20.0% Cr, and a boron content varying from 0 to 1.49% (Table I). These alloys were studied by performing experiments on each of the two phases present—the boride and the matrix. Following the presentation of these data is a section on the stress-rupture properties and another giving results of an examination of the fractured specimens.

Chemical Analysis

A brief examination of the results of the chemical analyses of the five initial heats shown in Table I, especially the boron analyses, seems worthwhile at this point. In choosing the most likely value for the boron contents of the five initial heats, the results from Laboratory C were neglected because on two of the samples, R311 and R308, values substantially in excess of the amount added to the heats were reported. All the boron determinations from this laboratory must therefore be regarded as doubtful, especially since the two other laboratories obtained results in quite good agreement with each other.

The carbon analyses on the five initial heats is essentially constant and well below the minimum value necessary to produce age-hardening phenomena.[6] Nitrogen analyses are at a constant low level. The oxygen level of heats R310 and R311 is somewhat higher than the other heats, a result which could be attributed to surface oxide. It should also be noted that zirconium was not reduced from the zirconia crucibles.

Boride Studies

The precipitate phase was studied by measuring its quantity, hardness, x-ray diffraction pattern, and chemical analysis. An attempt to synthesize the precipitate yielded an x-ray diffraction pattern very similar to that found in the experimental heats.

Quantity of Borides as a Function of Boron Content.—One of the most obvious effects of increasing the boron content in these alloys is an increase in the amount of boride phase present in the microstructure (Fig. 5). To differentiate this phase from other precipitates, the borides shown in Fig. 5 will subsequently be called gross borides. The amount of this phase in each of the heats obtained by point-counting methods (Table III) is shown by each photomicrograph. A tendency for the more rapidly cooled gage lengths of the tensile bars to have a greater amount of gross boride precipitate than the more slowly cooled ring gate metal was observed but is not considered significant in view of the errors inherent in the point-counting technique.

The appearance of the gross borides suggests that it was formed from a eutectic reaction.

Hardness of Borides.—Some of the boride particles in the 1.49% B heat were large enough to permit microhardness readings. The mean value of 25 readings was 1295 kg/mm^2 (Ludwik Vickers hardness). The maximum hardness observed in the set of 25 readings was 2360 kg/mm^2, and the 95%

confidence limits for the mean value can be expressed by the range 1160-1450 kg/mm^2. These values are within the range of published values for borides.[29]

X-Ray Diffraction Patterns.—The borides were extracted from specimens from the three highest boron heats and x-ray diffraction patterns were made. The results shown in the first three columns of Table IV can be compared with the patterns for Fe_2B, CrB, and Cr_2B. The d values of these correspond more closely than any other known phase to the observed patterns.

Chemical Analysis of Gross Boride from Heat R309.—Approximately 200 mg of the boride phase were separated from heat R309 (1.49% B) and submitted to Laboratory C for chemical analysis. Wet chemical methods yielded the following results.

Nickel:	1.90%	Density (pycnometric)
Chromium:	25.27	5.255 g/cc
Iron:	47.6	
Boron:	13.84	

A qualitative spectrographic anlaysis on the material showed, in addition to the above:

Ca	0.5	to 5.0%	
Al, Mn, Mo, Si	0.1	to 1.0%	each
Ti	0.05	to 0.5%	
Co, Cu	0.01	to 0.1%	
V	0.005	to 0.05%	
Fb, Sn	0.001	to 0.01%	each
Zn	0.0005	to 0.005%	
Bi, Cd, Mg, Sb	Not detected		

Unfortunately, these data are open to question not only because of the trouble experienced by Laboratory C with boron analyses, but also because only 88.6% of the boride was accounted for. It can be safely stated, however, that the gross borides are predominantly Fe-Cr borides.

Synthesis Experiments.—The results presented in the previous two sections indicate that the gross boride precipitate present in heat R309 was

not entirely either Cr_2B, CrB, or Fe_2B. The precipitate could be a mixture of two or more phases, but since it initially appeared to be a single phase under the microscope, it was reasoned that it might be a phase corresponding to the formula FeCrB. Heat R371 was made to this aim analysis, 33-1/3 atomic percent of each of the three elements, and found to have the microstructure shown in Fig. 6. Two boride phases as well as a small amount of excess Fe-Cr metallic phase at the grain boundaries were readily visible. The two boride phases could be distinguished unequivocally by their microhardnesses as shown below.

	Boride A	Boride B
Appearance in Fig. 6	Etched Dark Grey	Etched Light Grey
Ludwik-Vickers Hardness, kg/mm^2		
Lower 95% C.L.	2400	1930
Mean of 25 readings	2480	1985
Upper 95% C.L.	2575	2040

An x-ray diffraction pattern of crushed material from this heat corresponded very closely to the residues from heats R308, R309, and R312 (see Table IV).

After acquisition of these data, the borides in heats R308, R309, R311, and R312 were examined more closely at higher magnifications. Severe etching revealed what could reasonably be a duplex structure in some of the individual boride particles (Fig. 7). Some of the larger borides in Fig. 5d also appear to have a dual structure.

Matrix Properties

The austenitic matrix of the as-cast material in heats R308 through R312 was studied by measuring its hardness and lattice parameter.

Microhardness of Austenite.—The Ludwik-Vickers hardness of the austenitic phase increased from a value of approximately 132 kg/mm^2 in the 0% B heat

to nearly 155 kg/mm^2 in the 1.49% B heat as shown by the plot of data in Fig. 8. These values appeared to be quite reproducible as shown by readings on duplicate samples from each heat. The effect of preparing specimens improperly is shown by the upper curve in this illustration.

Lattice Parameter of Austenite.—The lattice constants of the as-cast austenitic matrices in this same series of alloys are represented by open circles in Fig. 9. The data given in this figure were obtained by the first method described earlier.

Stress-Rupture Properties

The 1500°F (816°C) stress-rupture properties of vacuum-melted heats R308, R309, R311, and R312 are presented in Table V. From log-stress versus log-rupture-time plots for each heat the stresses to produce rupture in 10 and 100 hr were obtained. These results, which are plotted in Fig. 10, show that the rupture strengths increased with boron content. Also shown on this figure are data for argon-melted heats made to the same aim analyses (see Table II). In general, no significant differences in rupture properties between the two types of melting procedures were observed.

Creep curves were obtained for many of the vacuum-melted specimens. The minimum second-stage creep rates in percent per hour derived from these curves are included in Table V.

Examination of Fractured Rupture Specimens

Longitudinal microspecimens were cut from the gage lengths of the fractured rupture specimens adjacent to the fractures. Microhardnesses were taken on these samples, x-ray diffraction patterns were obtained on the residues, and the lattice parameters were measured.

Microstructure of Fractured Rupture Specimens.—A metallographic examination of the fractures of all the stress-rupture specimens whose properties are given in Table V gave evidence that failure during a 1500°F (816°C) stress-rupture test apparently consists of three stages which may and probably do overlap one another.

Stage 1.—Realignment and/or rotation of the structure in such a way that the borides, which in the as-cast structure were oriented more or less randomly, tend to become aligned parallel to the tensile direction. This phenomenon is most evident in the lower boron heats.

Stage 2.—As creep proceeds, the austenitic matrix deforms, resulting in plastic flow in the direction of the applied load. The borides themselves, however, are quite brittle and many fracture. Also the matrix cracks between adjacent boride particles which have become aligned more or less parallel to the tensile direction. This condition is accentuated by the severe notch effect in the vicinity of two or more aligned boride particles.

Stage 3.—Finally, the matrix in the larger areas between columns of boride particles cracks along sub-grain boundaries and the specimen fails.

The photomicrographs of Fig. 11 illustrate the aligned borides (Stage 1), the cracks in and between aligned borides (Stage 2), and the sub-grain-boundary cracks in the austenite (Stage 3).

In addition to these effects, other microstructural changes were observed in the higher boron heats R308 and R309. In these two heats a general matrix precipitate was observed; typical examples are shown in Figs. 11c and 11d. To establish whether this precipitate might or might not involve nitrogen (or oxygen) from the air, vacuum-fusion analyses were run on a few samples. The results are shown below.

Heat No. and Boron Content	R308(0.80% B) %N	%O	R309(1.49% B) %N	%O
Gas content—As-cast	0.009	0.008	0.006	0.009
Gas content in sample adjacent to fracture of rupture specimen which showed general matrix precipitate	0.008	0.004	0.010	0.011
Gas content in sample obtained from unstressed portion of rupture bar (extensometer pins)	0.013	0.016		
Specimen number and duration of test from which samples were taken (see Table V)	No. 7, 64.5 hr		No. 7, 39.1 hr	

Very little precipitate of the type described above was observed in the 0.32% boron heat and none in the 0.10% B heat. Chemical analyses on one of the latter samples yielded the following results.

Heat No. and Boron Content	R311 (0.10% B) %N	%O
Gas content—As-cast	0.009	0.027
Gas content in sample adjacent to fracture of rupture specimen	0.031	0.035
Specimen number and duration of test from which sample was taken (see Table V)	No. 5, 400 hr	

Microhardness of Austenite in Fractured Rupture Specimens.—The matrix hardness of the 0.10 and 0.32% B heats was found to decrease during rupture testing while that of the 0.80 and 1.49% B heats (those which exhibited more pronounced precipitation during rupture testing) did not. These results are shown in Fig. 12.

X-Ray Diffraction Pattern on Residue from Fractured Rupture Specimen.—An x-ray diffraction pattern was prepared from the residue from one of the high boron heats which exhibited a general matrix precipitate after rupture-testing. The sample was prepared from a piece of the metal adjoining the fracture. It should be pointed out that the x-ray pattern so obtained was made on the same rupture specimen which was used for nitrogen and oxygen analysis (R308-7). Calculated d spacings for this sample are presented in Table IV where they can be compared with x-ray diffraction patterns on other residues.

Lattice Parameter of Austenite in Fractured Rupture Specimens.—The open square symbols on Fig. 9 denote the lattice parameters for a few samples in this condition [R311-5 (400-hr test), R312-8 (166-hr test), and R309-3 (112-hr test)]. Since no change from the as-cast condition was observed for the three specimens, it was not considered necessary to determine the lattice constant for all the specimens shown in Table V.

Heat-Treatment Investigations

Samples from the five initial heats were subjected to various single heat treatments to determine if the structure, microhardness, or other properties of the cast material might be altered. Following the description of these results is a section on the stress-rupture properties of heat-treated alloys and another which gives the results of an examination of the fractured stress-rupture specimens. This section is concluded with a brief resume of a series of aging experiments which were performed and a summary of the results of the diffusion experiments.

Effects of Single High-Temperature Heat Treatment

Small samples of the ring gates from the five initial heats were heat-treated for various lengths of time at temperatures of 2300, 2200, and

1500°F (1260, 1204, and 816°C). The data pertaining to microstructures, austenite hardness, and x-ray measurements are presented in that sequence.

Microstructural Changes Produced by Single Heat Treatments.—Before presenting these results, Fig. 5, which illustrates the as-cast structure of the alloys for different boron contents, may be recalled.

The microstructures of samples heat-treated at a temperature of 2200°F (1204°C) for 24 hr followed by an air cool are shown in Fig. 13. Perhaps the most apparent change produced by this heat treatment was the spheroidization of the borides which occurred. This process takes time. For example, the borides in a group of samples heat-treated for 6 hr at 2200°F (1204°C) were not spheroidized to nearly the extent of the 24-hr samples shown in Fig. 13. Samples heat-treated for equivalent lengths of time at 2300°F (1260°C) spheroidized more rapidly.

In addition to this spheroidization process, high-temperature heat treatments such as these also caused the formation of a general matrix precipitate in the 0.80 and 1.49% boron heat. It is obvious that the structures shown in Figs. 13c and 13d contain a fine precipitate within the austenitic grains, whereas the as-cast materials (see Fig. 5) do not. In both of these heats, but especially in the 0.80% B heat, the quantity of precipitate appeared to vary from one spot to another within the specimen. In the other two alloys, 0.10 and 0.32% B, no general matrix precipitate was noticed in any of the samples.

A third change in the microstructure appears to have taken place as a result of the high-temperature heat treatment. In general, the austenite grain boundaries were not observed in the as-cast condition but they were frequently quite noticeable after a high-temperature heat treatment (see Figs. 13a and 13c for examples).

A 1500°F (816°C) heat treatment for 100 hr followed by an air quench

produced only small changes in the microstructure of the specimens. A slight amount of general matrix precipitate was observed in the two higher boron heats. This precipitate was similar in appearance to that found in the samples just described, but it was not nearly as marked at 1500°F (816°C) as at the higher temperatures. No spheroidization of the boride and no grain-boundary delineation were noticed in the samples heat-treated at 1500°F (816°C).

To summarize the microstructural changes produced in these alloys by a high-temperature heat treatment [2200 to 2300°F (1204 to 1260°C)], it can be said that the heat treatment spheroidized the borides, caused the formation of a general matrix precipitate in the higher boron alloys, and developed the austenite grain boundaries. The precipitation within the austenitic phase was the only one of these three processes which occurred to any noticeable extent during a 1500°F (816°C) heat treatment. No difference was observed between air-cooled and water-quenched samples.

Microhardness of Heat-Treated Austenites.—Softening of the austenite to a level characteristic of the 0% B heat was the result of high-temperature heat treatments as shown in Fig. 14. The 95% confidence limits for the mean of 25 determinations are shown by the vertical lines through each point.

No data are presented for samples from heats R308 and R309 heat-treated at 2300°F (1260°C) since the specimens melted. Apparently the boride and/or austenite composition in the samples was different from that in the lower boron heats because all the specimens were heat-treated simultaneously.

X-Ray Diffraction Pattern on Residue.—A sample of precipitate from the 0.8% B heat which exhibited the general matrix precipitate after a high-

temperature heat treatment [2200°F (1204°C) for 24 hr, water-quenched] was prepared and the x-ray diffraction pattern determined. The results of this experiment, which are shown in Table IV, indicate that no new diffraction lines occur as a result of the high-temperature treatment.

Lattice Parameter of Austenite After High-Temperature Heat Treatment.— Experimental values determined by the first method of sample preparation are shown by special symbols in Fig. 9. A high-temperature heat treatment of filings—the second method of sample preparation—produced the results shown in Fig. 15. The curve of Fig. 9 is reproduced on Fig. 15 since the data on both graphs were obtained on samples from the same heats.

While measuring the films made by the first method, it was noticed that the 220 α_1 and 220 α_2 diffraction lines were much more distinct in the lower boron heats as compared to the higher boron heats. To obtain a more quantitative estimate of the breadth of the diffraction lines, microphotometer surveys of these doublets were performed. The width of the doublet at half height above the background was measured from the traces. The results given below are the averages of three different determinations.

Heat	%B	Width of 220 Doublet at Half Height, degrees in 2θ
R311	0.10	1.10
R312	0.32	1.20
R309	1.49	1.41

Qualitatively speaking, these data are not unique. In the series of films taken to determine the lattice parameter of the as-cast material, it was also noticed that the high-angle lines were more diffuse at high boron contents compared to those at low boron contents.

Stress-Rupture Properties of Heat-Treated Alloys

Although the exploratory heat-treatment studies just described were conducted at 2200°F (1204°C), it was necessary to heat-treat tensile specimens at a slightly lower temperature [2150°F (1177°C)] to prevent the threads of adjoining bars from sintering together. Other work[3] had shown that 2150°F (1177°C) would produce essentially the same microstructural and hardness changes observed at 2200°F (1204°C). If, on the other hand, the temperature were reduced below about 2000°F (1093°C), spheroidization of the borides, for example, would not occur nearly as rapidly.

The creep and stress-rupture data of heat-treated bars, as well as data on specimens in the as-cast condition from the same heats, are shown in Table VI. The second-stage creep rate was always less and the rupture life was usually extended by a 2150°F (1177°C) heat treatment. Typical examples are shown graphically in Fig. 16.

Examination of Fractured Rupture Specimens Tested After Heat Treatment

Microstructure of Failed Rupture Specimens.—In every microspecimen from a test bar which had been heat-treated prior to test (Fig. 17 shows typical examples), a fine precipitate was produced along sub-grain boundaries. The quantity of sub-grain-boundary precipitate varied in a random manner from sample to sample. It was most evident in the specimen cut from R344-7 (see Table VI). An electron micrograph from this sample, Fig. 18, revealed that the precipitate was comprised of a row of small idiomorphic crystals.

For purposes of comparison, the microstructures of bars, from the same heats whose structures are shown in Fig. 17 but from other bars which were tested in the as-cast condition, are shown in Fig. 19. No pronounced sub-grain-boundary precipitate was seen in these specimens nor in any

specimens from the initial heats (Fig. 11).

Microhardness of Austenite in Failed Rupture Specimens.--It has been shown previously that the high-temperature heat treatment softens the austenitic matrix (Fig. 14). No changes were produced in the hardness of the matrix as a result of stress-rupture testing the heat-treated specimens.

X-Ray Diffraction Pattern on Residue.--The interplanar spacings of the residue from the bromine treatment of specimen R395-3 (see Table VI and Fig. 17c) are included in Table IV. This residue sample presumably contained the sub-grain-boundary precipitate characteristic of stress-rupture bars which had been heat-treated prior to testing. Diffraction lines in addition to those of the gross boride precipitate were present

Aging Experiments

A group of samples from the five initial heats were heat-treated at 2200°F (1204°C) for 24 hr, water-quenched, and then aged at temperatures of 1400, 1550, and 1700°F (760, 843, and 927°C) for periods up to 100 hr. All the results confirm Cornelius' conclusions,[6] namely, that these alloys do not age-harden. In this case, furthermore, a more sensitive microhardness technique was used instead of Cornelius' gross Vickers hardness measurement.

Diffusion Experiments

In each of the specimens three distinct zones were noted (see Fig. 20). Zone A, the center zone, consisted of a mixture of a boride phase or phases plus metallic matrix. It was evident that metal had diffused into the center and boron had diffused outwards into the austenite. In both samples the diameter of zone A was considerably larger than the

original hole. Only a trace of porosity was detected. Zone B consisted of a relatively thin layer (.028 in. wide on the average) surrounding zone A in which isolated spherical particles of some other phase had formed. Zone C, the balance of the specimen, was characterized by a pronounced precipitate at the grain boundaries and sub-grain boundaries. This precipitate was similar in appearance to that formed when heat-treated test bars were rupture-tested (see Fig. 17).

Microhardness traverses were made across the samples by making impressions in the matrix at 0.10-mm (0.00394-in.) intervals. No change was observed across the specimens, and in fact the average of all readings agreed with the hardness of the as-cast alloy from which the samples were made within the limits of experimental error as shown below.

As-cast austenite hardness, R310, 95% C.L.:
129.7 - 134.8 kg/mm^2
Average austenite hardness of 2150°F (1177°C) diffusion sample, 95% C.L.:
127.3 - 134.4 kg/mm^2

Pre-Stressing and Heat-Treating Experiments

Although this research program was primarily concerned with cast alloys, a few experiments were conducted on alloys which had been cold-worked slightly by pre-stressing at room temperature in a tensile machine. Some of the specimens from heat R435 were rupture-tested after pre-stressing and others were heat-treated at 2150°F (1177°C) after pre-stressing and prior to rupture-testing.

It was found that pre-stressing increased the strength of the alloy and that the amount of strengthing varied, depending upon the amount of pre-stress and whether or not the bars were heat-treated. Data pertaining to this experiment are shown in Table VII, and in the curves of Fig. 21. The experiment is summarized below. Numbers of the figures which illustrate the structures of the broken rupture specimens are included.

Pre-Stress	Bars rupture-tested as Pre-Stressed		Bars Heat-Treated at 2150°F (1177°C) After Pre-Stressing and Before Rupture-Testing	
None	Bar 1	Fig. 19a	Bar 5	Fig. 17a
0.4%	Bar 6	Fig. 22a	Bar 2	Fig. 22b
1.2%	Bar 3	Fig. 22c	Bar 7	Fig. 22d

Bars from a companion heat, R434, were given the same series of pre-treatments and examined without rupture-testing. The data on nonheat-treated samples showed that pre-stressing had hardened the matrix slightly (approximately 5 points on the Ludwik-Vickers scale), as anticipated. Heat treatment had spheroidized the gross borides. Presumably, then, the bars from heat R435 were in an identical condition prior to testing.

DISCUSSION OF RESULTS

This discussion of the experimental results is divided into several categories. The as-cast material is considered first, after which attention is directed towards the effects of heat treatment. The mechanical property data can be reviewed and interpreted more meaningfully against this background. Finally, these findings are related to published work.

As-Cast Material

One of the most obvious effects produced by adding boron to iron-nickel-chromium austenites is the formation of a boron-rich precipitate in the microstructure. The data pertaining to this phase are examined first and then those applying to the matrix phase are reviewed.

Boride Phases

There is certainly no question that the gross precipitate phase or phases are borides, but there is some doubt concerning their exact nature. Chemical analysis revealed the presence of substantial quantities of iron and chromium in the precipitate from the 1.49% B heat (R309), but the analysis did not correspond to any simple stoichiometric ratio.

A study of the x-ray diffraction patterns shown in Table IV revealed that the precipitate was most likely a mixture of Fe_2B, CrB, and Cr_2B, and that the lower boron heats were relatively richer in Fe B and Cr B while the higher boron heats probably contained more Cr_2B. This can be seen from the summaries on the following page.

a) X-ray diffraction data pertaining to Fe_2B

Lines Attributable to Fe_2B	Line No. from Table IV	d Values and Relative Intensities for samples: R312 - 0.32% B	R308 - 0.80% B	R309 - 1.49% B
2.55 wm	11	2.515 s	2.56 vw	2.54 vvw
2.13 wm	17	2.169 vvw		
1.38 w	37	1.385 m	1.383 vw	
1.345 ms	38	1.372 m	1.374 vw	1.373 vvw
1.205 m	50	1.204 w	1.202 s	1.201 m
1.19 s	51	1.182 vs	1.184 s	1.182 m

b) X-ray diffraction data pertaining to CrB

Lines Attributable to CrB	Line No. from Table IV	d Values and Relative Intensities for samples: R312 - 0.32% B	R308 - 0.80% B	R309 - 1.49% B
4.35 s	1	4.25 w	4.20 vvw	
2.74 m	9	2.805 w		
2.61 s	10	2.652 w		
2.49 vs	12	2.464 w		
1.46 m	34	1.461 vvw		
1.43 s	35	1.428 vw		

c) X-ray diffraction data pertaining to Cr_2B

Lines Attributable to Cr_2B	Line No. from Table IV	d Values and Relative Intensities for samples: R312 - 0.32% B	R308 - 0.80% B	R309 - 1.49% B
2.038 vvs	21	2.025 s	2.031 vs	2.017 vs
1.950 m	23	1.949 w	1.943 m	1.936 w
1.821 s	26	1.810 m	1.813 s	1.804 s
1.649 vs	30	1.635 m	1.637 s	1.631 s

The conclusion regarding Cr_2B must be tempered somewhat by the fact that some of the strong lines of the Cr_2B pattern were not observed in the residues (lines 18?, 42, 46, 48, and 52). On the other hand, these lines may have been caused by the presence of another phase in the sample, for example, a higher boride.

One of the conclusions developed in the preceding paragraph is that the borides occurring in the experimental heats are very probably a mixture of Fe_2B, CrB, and Cr_2B. Additional evidence that the gross precipitate is not a single phase is seen in the close similarity between the x-ray patterns of the residues and that of the heat made to an aim analysis corresponding to FeCrB, heat R371. This heat definitely contains more than one boride phase as determined by metallographic examination (Fig. 6) and microhardness measurements. Finally, the dual nature of many of the individual gross boride precipitate particles was observed in some of the experimental heats (Figs. 5d and 7).

Supplementary support of the premise that the relative amounts of the various borides varies from heat to heat is obtained by plotting the density of the alloys versus boron content (Fig. 23). If the relative amounts of the various phases remained the same at different boron levels, this curve should be a straight line. The fact that the points fit the shown curve better than any straight line is therefore a further indication that the composition of the borides varies.

The hypothesis that the relative amounts of the various boride phases change with composition can be substantiated further. This involves the lattice-parameter measurements of the austenite phase, which are discussed next.

Austenitic Phase

The curves of Fig. 9 and Fig. 15* illustrate how the lattice parameter of the austenite in the five original heats varies with composition for two different methods of sample preparation. At first glance, it may seem that the curves show that boron dissolves sometimes substitutionally, sometimes interstitially, and that the lattice parameter of the austenite therefore varies in an irregular fashion. Chromium and/or iron-rich borides are also formed, however, as boron is added. The atomic diameter of these two elements is greater than that of the third major component of the austenite, nickel. Thus as more borides are formed, a greater amount of the larger atoms is removed from the matrix and the lattice parameter therefore decreases. This effect can, in principle, be calculated by employing a material balance and Vegard's law. In practice, however, the chemical analysis of the boride is dubious so that certain assumptions concerning the probable errors must be made.

If it is assumed, firstly, that the boron analyses on the experimental heats are more reliable than the boron analyses on the boride, and secondly, that the difference between the sum of actual analyses on the boride and 100% is prorated to the nickel, chromium, and iron contents of the boride, then the lattice constant of the 1.49% B heat is calculated as 3.580 Å using the data of Fig. 9 (see Appendix II). This should be compared with a measured value of 3.583 Å. A similar calculation using as a basis the value of the lattice constant for heat R310 from Fig. 15 produces a similar result. The measured value of the lattice parameter of the 1.49% B heat is about 0.004 Å greater than the calculated value.

*These graphs will be discussed more fully later. Only the curves themselves are considered here.

If, on the other hand, it is assumed, firstly, that the relative amount of Ni, Cr, Fe, and B in the boride as determined by chemical analysis is substantially correct, and secondly, that the difference between the total amount accounted for by analysis (88.6%) and 100% is prorated among the four elements, then the calculated lattice constant for the 1.49% B heat checks the measured value much more closely. This set of assumptions, however, leads one to the irreconcilable paradox that the boride of heat R309 contains almost twice the amount of boron actually added.

Each of these calculations is quite strongly dependent upon the density of the boride, which was determined experimentally as 5.255 g/cc. This value is considerably lower than the reported values for Fe_2B, CrB, and Cr_2B.[29] In spite of these difficulties and uncertainties, however, the calculations show that the changes in austenite composition are of such a magnitude that they could logically account for the changes in lattice constant which were observed. If the more reasonable* set of assumptions—the first set—is accepted, the calculations reveal in addition that boron is dissolving interstitially in austenite.

With these statements in mind, the fact that the curves of Fig. 9 and/or Fig. 15 are nonlinear is construed to mean that the borides which are formed are of varying composition. If, to argue from the other side, the borides in the various heats differed only in quantity and not chemistry, then the curves should be linear. Indeed the shape of the curve qualitatively verifies the conclusions which have been reached regarding the composition of the phases. This can be seen by observing that one

*More reasonable because two laboratories agree on the boron analysis of the heats, because the irreconcilable paradox (of having more boron present than was added) is absent, and because less reliance is placed upon the questionable chemical analyis of the boride.

atom of boron will decrease the lattice constant of austenite most if it removes two atoms of the largest element, chromium, from the matrix (Cr_2B). A lesser effect will be produced if one atom of boron removes two smaller atoms (Fe_2B) or only one of the large atoms (CrB). The peak in the curves in the vicinity of 0.30% B, and the sharp drop-off at higher boron contents is therefore considered as further confirmation that the borides found at low boron levels are, relatively speaking, richer in Fe_2B and/or CrB, while those formed at the higher boron contents are richer in Cr_2B.

Effect of Heat Treatment

The data regarding the precipitate phases will again be discussed first, and then those pertaining to the matrix.

Precipitate Phases

Fine precipitate phases which have been produced as a result of heat treatment or rupture-testing are discussed here. These results should not be confused with those pertaining to the gross boride precipitates.

Produced by Heat Treatment.—The high-temperature heat treatment which was employed to enhance the 1500°F (816°C) rupture properties did not cause the appearance of any new phases as determined by x-ray diffraction techniques. Even when the 2200°F (1204°C) heat treatment produced a fine general matrix precipitate (the 0.80 and 1.49% B heats, see Figs. 13c and 13d), no new diffraction lines were observed (compare x-ray pattern on residues from as-cast and heat-treated samples from heat R308 in Table IV). The 2200°F (1204°C) heat treatment, provided its duration was at least 20 hr, spheroidized the borides, however. Evidently the fine precipitate observed in the higher boron heats was just a finely coalesced form of the precipitate present in the as-cast structure.

Produced by Rupture-Testing.—Heat treatment of the alloys under stress—that is, stress-rupture testing at 1500°F (816°C)—did cause the appearance of new diffraction lines. It will be recalled that a fine general matrix precipitate was observed in the microspecimens cut from the fractured gage lengths of the higher boron heats which were rupture-tested in the as-cast condition (Figs. 11b, 11c, 11d, 19b). Also a sub-grain-boundary precipitate was noticed in all specimens cut from fractured rupture bars which were heat-treated prior to test (Figs. 17a, 17b, 17c). It should be emphasized that the latter phenomenon occurred at boron levels from 0.1 to 1.0%.

The diffraction data on residue samples characteristic of these two conditions are shown in the last two columns of Table IV. The new diffraction lines appearing in these samples are summarized below.

Identification No. in Table IV	Diffraction Lines Not Present in As-Cast Samples		Excess Strong Cr_2B Lines
	Sample Characteristic of General Matrix Precipitate, R308-7	Sample Characteristic of Sub-Grain-Boundary Precipitate, R395-3	
13	2.400 vw	2.366 vvw	2.381 vvw*
16	2.233 vvw		
18	2.114 vs		2.107 vvs
20		2.038 w	2.038 vvs**
24	1.874 vw	1.870 vw	CrB line
27		1.790 vvw	
42	1.268 m		1.263 s
46	1.225 w	1.226 w	1.224 vvs
48			1.214 vs
52	1.161 s	1.166 vw	1.165 vs

*Not strong.
**Not excess.

The last column in the above table shows the interplanar spacings of relatively strong lines observed in the sample of Cr_2B which were not observed in the residues from the as-cast samples. They have been labeled "Excess Strong Cr_2B Lines."

There is little question that the combined action of stress and temperature [1500°F (816°C)] has caused the appearance of a new phase or

phases in view of this x-ray diffraction evidence and at new locations as shown by the metallographic evidence. A similarity between the two sets of lines and a synthetic chromium boride in the preceding tabulation as well as other similarities* and correlations** suggests very strongly that the precipitate phase (or phases) is a boride. The results are not sufficiently clear to permit incontrovertible identifications to be made nor to say with certainty whether the two types of precipitate are the same or different. It is suspected, however, that the general matrix precipitate is similar, in some features, to the sub-grain-boundary precipitate.

Matrix Changes During Heat Treatment

The experimental results shown in Figs. 9 and 15 will now be considered in more detail. The hardness data will then be reviewed.

Lattice Parameter.—It has already been shown that the change in lattice parameter with boron content can be attributed to varying austenite composition. In this section the relation between the two curves and among the various points from the same heat on either graph are discussed.

Referring first to Fig. 9, it is noted that there is no systematic trend among the various types of points shown. That,is, all the observations for any one heat check with one another within limits of about ± 0.0002 angstrom units. The data in Fig. 15 follow a similar pattern: the 1300°F (704°C) heat treatment did not influence the lattice parameter [as determined after the 2150°F (1177°C) treatment]. There is, however,

*Lines 10 and 17 are boride lines common to R308-7 and R395-3 observed in some but not all the as-cast samples.

**Lines 12, 29, 34, 35, and 37 are boride lines seen in R308-7 and in some but not all the as-cast samples. Lines 4, 25, 28, and 39 are boride lines seen in R395-3 and in some but not all the as-cast samples.

a real difference between the absolute values of the lattice parameters plotted in the two illustrations. It may be that all the values shown in Fig. 9 are lower than the true values because of boron precipitation from the austenite during filing and annealing. Or the difference between Figs. 9 and 15 may be associated with some type of surface reaction which occurs at a high temperature. Such a surface reaction would not be detected with the first method of sample preparation, Fig. 9, and could not be avoided with the second method, Fig. 15. Deboronization, reaction with the quartz tubing, or reaction with adsorbed films of some type on the surfaces of the filings are all reasonable possibilities which could account for this anomaly.

Although it seems that heat treatment or rupture-testing does not alter the lattice parameter, this conclusion must be viewed cautiously. As pointed out previously, the difference between the data shown in Figs. 9 and 15 is logically attributable to (surface) reactions which occurred when filings were heat-treated at a high temperature for a long time or to precipitation reactions as a result of cold-working and annealing. Apart from this change, though, all the points for any given heat on either graph do seem to illustrate that the lattice parameter is insensitive to heat treatment or rupture-testing. This may be the case. It may also be that the lattice parameter does change with heat treatment or rupture-testing but that such effects are not pronounced in strain-free material at 1300°F (704°C), as shown by the data of Fig. 15. This detail could not be resolved because it was necessary to use filings to evaluate the lattice parameter with sufficient precision.

Regardless of this paradox, the data shown in Figs. 9 and 15, taken singly or together, do demonstrate, by the nonlinearity of the curves, that the Cr, Ni, and Fe content of the austenite varies in an irregular fashion

with boron. Therefore, since the alloys are of similar total composition, the composition of the borides also varies with boron content.

Hardness Data.—The results of the microhardness measurements shown in Fig. 14 require little interpretation. It should be pointed out, though, that the softening process was by no means an instantaneous one.

Mechanical Properties

Gross borides certainly influence the room-temperature properties very markedly by their adverse effect on ductility. At 1500°F (816°C) in short-time tensile tests, lack of ductility does not appear to be a severe problem (Fig. 10). Somewhere between room temperature and 1500°F (816°C) for short-time tests, the temperature region would be found where it would be difficult to decide whether the matrix or the gross borides governed the properties. On the other hand, it has been demonstrated, on several heats at boron levels from 0.10 to 1.0%, that a high-temperature heat treatment prior to rupture-testing invariably reduces the second-stage creep rate of cast austenitic alloys (Table VI) without changing the amount of gross boride precipitate. Usually also an improvement, frequently quite substantial, is noted in rupture life. Examination of failed stress-rupture specimens has disclosed that the gross borides can and do realign during test. In other words, fracture is limited by the matrix. These facts show that it is the matrix, as contrasted with the gross boride precipitate, which governs the creep-rupture properties. As an outstanding example of the range of creep-rupture properties that can be produced in an alloy with a constant amount of gross boride precipitate, attention is recalled to the data of the pre-stressing experiment, Fig. 21.

Interpretation of Results

It has just been shown that the austenitic matrix, not the gross boride precipitate, governs the creep-rupture properties of these cast alloys at 1500°F (816°C). Therefore, since the higher boron heats are consistently stronger than the lower boron heats, the improved properties must be associated with boron present in the matrix.

A study of the microstructure of failed stress-rupture specimens tested in the as-cast condition (Figs. 11 and 19) shows that fracture occurs within the austenite grains and that a visible general matrix precipitate occurs, at least in the higher boron alloys. Some tendency for this precipitate to arrange itself into a cellular pattern is observed. Now the alloys which have been given an extended 2150°F (1177°C) heat treatment prior to rupture-testing show a much more pronounced sub-grain-boundary precipitate after testing (Fig. 17). This is found at boron levels from 0.1 to 1.0%. Invariably the alloys exhibiting this are stronger. Metallographic and x-ray diffraction data on residue samples have revealed that these precipitates do not form during solidification or heat treatment, but during rupture-testing. Both precipitates, however, are of the boride type because of the similar diffraction lines. This is considered to be persuasive evidence that boron in the matrix strengthens the as-cast austenites through the formation of a precipitate along sub-grain boundaries during stress-rupture testing.

As-cast, the heats with a high boron content must have a greater potential for this kind of reaction than the lower boron heats because, *ipso facto*, they are stronger. This difference in potential could logically arise from at least two sources, both of which may be operative in these alloys.

The first of these derives from the fact that the borides formed at different boron levels vary in composition. In general, therefore, the activity of the boron in solution will vary depending on the nature of gross precipitate phases. A partition effect between boron as gross boride and boron in the austenite could thus be established, the concentration—activity, to be more rigorous—of boron in the matrix increasing with total boron content.

Another reasonable explanation for the aforementioned potential difference between heats with different boron contents may involve the casting process itself. During mold-cooling the test bars contract more than the silica-base investment molds because of the difference in coefficient of thermal expansion. This difference in contraction would cold-work the metal somewhat, thus introducing dislocations.* It seems logical to assume that the higher boron heats would have a higher dislocation density as a result of this process because of the presence of a larger quantity of hard, brittle boride particles in the structure. Boron atoms, because of their size, would tend to segregate to the dislocations; and since a greater dislocation density is postulated as occurring in the high boron alloys, a greater potential for precipitation during stress-rupture testing is present.

With either of these models, the net result is similar, namely, a higher boron content in the austenite at higher boron levels. With the research tools presently available, it is not possible to prove directly—without any ambiguity in interpretation—exactly where individual boron atoms are located within the austenite. It seems entirely logical, though,

*Dislocations will of course also be introduced during solidification, and as a result of any solid-state reactions which might occur during cooling. These mechanisms would just add to the effect described above.

to assume that a large proportion of the boron atoms will be associated with dislocations in the as-cast alloys. Obviously there will also be a high concentration at the sub-grain and grain boundaries. This postulate has been adopted here. There may in addition be some solid solubility, but the evidence (material balance calculation) does not support this.

The circumstantial evidence to support the postulate which has been adopted will now be reviewed. It is proposed that during rupture-testing of the as-cast material, the dislocations, with associated boron atoms, will tend to migrate to low-energy sinks in the structure. Here a large concentration of boron atoms appears and a new precipitate phase, which has many indications of being a boride of Cr and/or Fe and/or Ni forms. Some of this precipitate undoubtedly occurs at sub-grain boundaries (Figs. 11c, 11d, 19b), but most of it occurs at more or less random locations throughout the austenite. With this model, the higher boron heats would be expected to be stronger because of the greater number of dislocations with associated boron atoms which retard the movement (glide primarily[46]) of the dislocations through the metal. The sub-brain boundaries are still the weak points in the alloy, however.

To continue with this description of the postulated model, it is thought that an extended high-temperature heat treatment prior to rupture-testing would cause the dislocations, with the associated boron atoms, to move in such a way that rather well-defined (but not necessarily always visible) grain and sub-grain boundaries are formed. Evidence for this is found in the more sharply defined grain boundaries after such a heat treatment (Figs. 13a and 13c, for example). Any precipitate which might form as a result of this process would most likely be of the same type as the gross boride precipitate since it has been heat-treated for a long time at a high temperature to approach equilibrium (this also has been observed).

Also, the hardness of the austenite might logically decrease during heat treatment because the effect which caused the high boron heats to be harder—the dislocations with associated boron atoms—has been removed to the grain and sub-grain boundaries. However, since a multicomponent system is involved, this is uncertain. The softening phenomenon has been observed (Fig. 14).

Sub-grain and grain boundaries rich in boron are the consequences of a high-temperature heat treatment according to the model which has been proposed. The diffusion data confirm this in a qualitative way for it has been demonstrated that boron diffuses rapidly at these temperatures and tends to segregate at the grain and sub-grain boundaries (Fig. 20c). (It must be remembered that in these experiments the activity of the boron in the source for diffusion was that of elemental boron which probably accounts for the more visibly pronounced precipitate.) When alloys in this condition are rupture-tested, the weak points in the structure—the sub-grain boundaries—are now no longer as weak. All the creep-rupture data, in fact, confirm that alloys so heat-treated are stronger (Table VI) and the precipitate which occurs during testing shows pronounced tendencies to form along what are presumably sub-grain boundaries.

Cold-working by pre-stressing in a tensile machine introduces many more dislocations into the metal, probably orders of magnitude more. These additional dislocations strengthen the alloy (Fig. 21) as anticipated from the proposed model. The results of the exploratory experiments shown on this graph demonstrate that there apparently is an optimum amount of pre-stressing. The data also show that the high-temperature heat treatment actually impairs the stress-rupture properties of cold-worked metal. Obviously these few data are not sufficient, nor

were they intended to be sufficient, to delineate the complex interactions between strain, strain rate, recovery, recrystallization, grain versus grain boundary strength, boron content, and the relative effect of all these variables on the creep-rate and/or rupture-life of cold-worked alloys. The data do show that, when the added variable of cold-work is introduced, a study of the role of boron becomes more complicated for the reasons listed. In the cast alloys, though, the limiting feature which governs strength appears to be the strength of the sub-grain boundaries. This is not always the case in worked alloys. For example, bar 6, heat R435, was the strongest of the group, had significantly less ductility and reduction of area in the rupture test, and apparently failed by a different mechanism from that of the as-cast alloys, Fig. 22a.

Relation of Proposed Mechanism to Published Information

The model proposed in the foregoing discussion for these boron-containing alloys can be supported by published data for other systems. For example, the concept of strengthening by precipitation during the creep processhas been reported before. Glen[47] showed that, at high temperatures, normalized steels in which molybdenum carbides were allowed to precipitate during creep testing had a greater creep resistance than steels in which the carbides were precipitated prior to testing by a tempering treatment. This was considered to be a strain-aging reaction. These experiments and others were reviewed by Cottrell[46] who stated that precipitation on dislocations (and small-angle grain boundaries) during creep may be an important factor contributing to creep resistance.

It is frequently assumed that only extremely fine precipitate particles are effective in promoting strength, but Grant and Chaudhuri[48] have shown that relatively coarse precipitate particles (in this case produced

by overaging a 2% Cu-Al alloy) at the grain boundaries can retard grain-boundary migration during creep, whereas finer, more closely spaced particles do not. It may be that this retardation effect on sub-grain-boundary migration is also involved in the present case since the particles which have been observed as being effective in promoting strength are quite large.

CONCLUSIONS

A series of cast iron-base austenitic alloys containing boron in amounts from 0 to 1.49% has been studied with the objective of determining why such large amounts of boron are effective in promoting the rupture strength in view of the fact that much smaller amounts have been observed to be effective in wrought alloys.

The gross borides, which form in these alloys in significant quantities at high boron levels, vary in composition as the boron content is changed as shown by four types of experiments: x-ray diffraction patterns on samples of the borides prepared by bromine extraction, density measurements, lattice-constant determinations on the austenite, and heat-treating experiments. Although the borides have profound effects on the room-temperature tensile properties, it has been proven that the austenitic matrix controls the 1500°F (816°C) creep-rupture properties. Therefore, since the higher boron alloys consistently have better rupture properties than the heats with less boron, the austenite in these high boron heats must have a greater strength. Evidence has been presented which strongly suggests that the strength of the austenite arises from precipitation, during rupture-testing, of boron compounds in the matrix. This precipitation is accentuated, especially at sub-grain boundaries, with consequent improvement in the 1500°F (816°C) strength of the cast alloys by a high-temperature [2150°F (1177°C)] heat treatment prior to test. Evidently, in the cast alloys, a partition effect between boron as boride and boron in the matrix occurs. The difference in boride composition at different boron levels and/or the mere presence of a large amount of

a hard, brittle microconstituent in the high boron heats during casting are suggested as reasonable processes by which this partition effect is achieved.

A mechanism, akin to strain-aging, consistent with the known behavior of boron in ferrous alloys, satisfactorily accounting for the experimental observations, and having antecedents in the literature, has been proposed.

TABLE I

CHEMICAL ANALYSIS OF FIVE INITIAL HEATS

Heat No.	R310	R311	R312	R308	R309
Aim Boron - Wt. %	0	0.1	0.5	1.0	2.0
Chemical Analysis: Wt. %					
Boron - Laboratory A	0	.11 and .12	.33	.72	1.45 and 1.50
Laboratory B	0	.07	.30	.88	1.53
Laboratory C	.012	.198	.333	1.37 and 1.51	1.79 and 2.01
Most probable value	0	.10	.32	.80	1.49
Nickel	18.26	18.42	18.51	18.68	18.66
Chromium	20.73	19.96	19.98	19.80	19.00
Carbon	.03	.05	.04	.04	.04
Nitrogen	.004	.009	.007	.009	.006
Oxygen	.044	.027	.011	.008	.009
Qualitative Spectrographic Analysis:					
Silicon	--	.X	.X	.X	.X
Manganese	--	.X	.X	.X	.X
Copper	--	.X-low	.X-low	.X-low	.X-low
Aluminum	--	.X-low	.X-low	.X-low	.X-low
Molybdenum	--	.0X	.X-low	.X-low	.X-low
Vanadium	--	.0X	.0X	.0X	.0X
Cobalt	--	.0X	.0X	.0X	.0X
Tin	--	.0X-low	.0X-low	.0X-low	.0X-low
Zr,Nb,Ta,W,Pb, Zn,Sb,As,Bi,Ti	--	None of these elements found in any of these four heats.			
Physical Data:					
Density gm/cc	7.954	7.961	7.937	7.814	7.755
Volume percent boride	0	4.36	9.92	23.32	34.74

Note: All these heats were made using Armco iron as a source of iron.

TABLE II

SUMMARY OF ALL HEATS STUDIED

Group or Purpose	Heat Number	Type of Melting Furnace	Aim Analysis*
Five Initial Heats	R310	Vacuum	0
	R311	Vacuum	0.1% B
	R312	Vacuum	0.5% B
	R308	Vacuum	1.0% B
	R309	Vacuum	2.0% B
Argon-melted equivalent to preceding series	R40	Argon	0
	R105	Argon	0.5% B
	R180	Argon	1.0% B
	R192	Argon	2.0% B
Boride Synthesis	R371	Argon	33-1/3 atom. % each of Fe, Cr, and B
Tensile bars for heat treating and prestressing and heat-treating investigations	R394	Vacuum	0.1% B
	R418**	Vacuum	0.1% B
	R419**	Vacuum	0.1% B
	R434**	Vacuum	0.1% B
	R435**	Vacuum	0.1% B
	R344	Vacuum	0.5% B
	R396**	Vacuum	0.5% B
	R395	Vacuum	1.0% B

*Aim analysis and alloy charged for nickel and chromium was the same on all heats (except R371). The actual analysis on five such heats is shown in Table I.

**Heats melted using electrolytic iron rather than Armco iron.

TABLE III

BORIDE CONTENT OF FIVE INITIAL HEATS
POINT-COUNTING RESULTS

Boron Heat No.	0% B R310		0.1% B R311		0.32% B R312		0.80% B R308		1.49% B R309	
Location of Specimen*	GL	RG	GL	RG	GL	RG	GL	RG	GL	RG
Number of points out of 25 counted as boride. 0	200	200	75	95	19	25	1	6		
1			72	60	38	25	4	11		
2			31	26	49	45	13	33	1	3
3			15	14	48	38	21	42	3	7
4			2	4	25	39	28	33	9	19
5			1	0	14	15	30	27	11	17
6			3	1	4	11	29	26	18	22
7					2	1	30	13	25	25
8			1		1	1	13	7	33	28
9							11	2	33	33
10							9		27	24
11							6		14	11
12							2		7	8
13							2		8	3
14									4	
15									3	
16										
17									1	
18							1		1	
19										
20									1	
21										
22										
23									1	
Total Count	200	200	200	200	200	200	200	200	200	200
Mean Converted to % Boride	0	0	4.36	3.52	9.92	10.82	23.32	15.82	34.74	30.24

*GL: Gage length of tensile specimens
RG: Ring gate from heat

TABLE IV

X-RAY DIFFRACTION PATTERNS OF BORIDES
(Experimental data obtained on residues from bromine extraction.)
Tabular entries are d values in angstrom units and relative intensities.*

No.	As-Cast Precipitate			Identification Patterns				Heat-Treated 2200°F (1204°C) for 24 hr	Rupture-Tested As-Cast	Heat-Treated and Rupture-Tested
	R312, 0.32% B	R308, 0.80% B	R309, 1.49% B	R371	Cr_2B**	CrB[31]	Fe_2B[28]	R308, 0.80% B	R308-7, 0.80% B	R395-3, 1.0% B
1	4.25 w	4.20 vvw				4.35 s				
2	4.04 w									
3	3.618 vw	3.65 m	3.61 vw	3.63 w	3.65 w		3.62 vw	3.606 vw	3.63 m	3.632 w
4		3.56 vw		3.53 w	3.57 w			3.528 vvw		3.539 vw
5		3.48 vvw	3.52 vvw							
6	3.333 vs	3.35 m	3.32 vw						3.31 vw	3.325 vvw
7					3.03 vvw					
8	2.947 vvw	2.92 m	2.92 m	2.91 w	2.93 m			2.906 vw	2.93 w	2.914 vw
9	2.805 w			2.76 vw	2.71 vvw	2.74 m				
10	2.652 w					2.61 s			2.66 m	2.667 vw
11	2.515 s	2.56 vw	2.54 vvw		2.504 vw		2.55 wm	2.512 vvw	2.516 s	2.502 vw
12	2.464 w					2.49 vw			2.477 vvw	
13					2.381 vvw				2.400 vw	2.366 vvw
14				2.34 w	2.356 vw	2.36 w				
15	2.270 vs	2.284 vs	2.27 s	2.27 s	2.286 vs			2.269 s	2.273 s	2.270 s
16									2.233 vvw	
17	2.169 vvw						2.13 wm		2.166 vw	2.160 w
18					2.107 vvs	2.10 ms			2.114 vs	
19	2.089 s	2.097 vs	2.084 vs	2.083 vs		2.09 vs		2.085 s	2.089 vs	2.086 s
20										2.038 w
21	2.025 s	2.031 vs	2.017 vs	2.020 vvs	2.038 vvs	1.99 vw	2.01 vs	2.021 vs	2.023 vvs	2.018 vs
22				1.958 w	1.965 w	1.96 vw				
23	1.949 w	1.943 m	1.936 w	1.933 m	1.950 m			1.935 w	1.940 w	1.934 w
24						1.90 w			1.874 vw	1.870 vw
25		1.827 w	1.820 vw	1.823 w	1.841 m	1.84 vw	1.84 w	1.819 vw		1.821 vvw
26	1.810 m	1.813 s	1.804 s	1.802 m	1.821 s		1.815 w	1.807 s	1.806 s	1.804 s
27										1.790 vvw
28		1.742 vvw			1.720 w					1.767 vvw
29	1.668 w				1.678 vw	1.67 w			1.670 w	
30	1.635 m	1.637 s	1.631 s	1.633 s	1.649 vs	1.63 vs	1.64 ms	1.634 m	1.635 s	1.632 s
31	1.604 w	1.603 vw	1.604 vvw			1.60 s	1.615 ms		1.605 vvw	
32	1.540 vw									
33	1.480 w	1.480 m	1.476 w	1.477 vw	1.489 w	1.48 m		1.480 w	1.475{m diff.	1.480 w
34	1.461 vvw					1.46 m			1.451 vvw	
35	1.428 vw			1.427 vw		1.43 s			1.429 vw	
36						1.41 vw				
37	1.385 m	1.383 vw			1.391 vvw		1.38 w		1.387 m	
38	1.372 m	1.374 vw	1.373 vvw	1.374 vvw	1.344 vw		1.345 ms			
39			1.330 vvw	1.329 vvw	1.336 vw	1.30 vw				1.327 vvw
40	1.292 m	1.291 s	1.292 m	1.288 m	1.300{s diff.	1.29 w		1.292 m	1.292 m	1.291 m
41	1.289 vvw	1.287 w	1.287 w			1.28 mw	1.28 wm	1.288 w		1.285 w
42					1.263 s				1.268 m	
43	1.251 w	1.251 w	1.250 w	1.255 w	1.256 s			1.253 w	1.251 m	1.251 m
44	1.248 w	1.248 m	1.247 m	1.246 s	1.240 w			1.249 m	1.248 m	1.247 w
45					1.230 w					
46					1.224 vvs				1.225 w	1.226 w
47	1.218 s	1.215 vvs	1.214 vs	1.213 vs	1.219 s			1.216 vvs	1.215 vvs	1.214 vvs
48					1.214 vs					
49	1.206 vw	1.207 w	1.205 vw	1.200{vvs diff.	1.209 s	1.21 s	1.21 s	1.207 vw	1.207 vw	1.206 vw
50	1.204 w2	1.202 s2	1.201 m2				1.205 m	1.203 s2	1.205 vs2	1.202 m2
51	1.183 vs2	1.184 s2	1.182 m2	1.180 m2	1.192 m2		1.119 s	1.183 m2	1.181 m2	1.182 w2
52				1.163 m2	1.165 vs2				1.161 s2	1.166 vw
53	1.156 w2	1.154 m2	1.155 m2		1.160 vs2			1.154 m2	1.156 w	1.154 w

*s - strong, m - medium, w - weak, v - very, 2 - doublet, diff. - diffuse.

**Cr_2B pattern determined experimentally on material supplied by Steinitz.[32]

TABLE V

MECHANICAL PROPERTY DATA ON HEATS R308, R309, R311, R312

Heat No.	Boron, %	Bar No.	Test Temp., °F*	Load, psi	Life, hr	Elong., %	Red. of Area, %	Min. 2nd Stage Creep Rate, %/hr
R311	0.10	1	1500	16,900	STTT**	50.0	68.0	--
		3	1500	10,000	4.4	34.0	63.5	
		4	1500	8,000	23.2	40.0	66.5	1.4
		5	1500	6,000	400	31.0	48.0	.048
		6	70	63,200	STTT	26.0	46.0	--
R312	0.32	1	1500	11,000	11.3	36.0	55.0	
		7	1500	8,500	86.0	30.0	55.5	.174
		8	1500	6,800	166	46.0	65.0	
R308	0.80	2	1500	29,400	STTT	29.0	38.0	--
		3	1500	15,000	8.0	31.0	48.5	
		7	1500	12,000	64.5	16.0	35.0	.177
		6	1500	10,000	175	27.5	38.5	.064
		8	70	68,900	STTT	5.0	6.0	--
R309	1.49	8	1500	38,200	STTT	12.0	14.5	--
		1	1500	20,000	11.3	23.0	24.5	
		7	1500	16,000	39.1	13.0	30.0	
		3	1500	13,000	112.3	20.0	26.0	.057
		6	70	67,700	STTT	2.0	1.0	--

*1500°F = 816°C and 70°F = 21°C.
**STTT - Short-time tensile test.

TABLE VI

CREEP AND STRESS-RUPTURE DATA ON ALLOYS HEAT-TREATED AT 2150°F (1177°C)
[All tests conducted at 1500°F (816°C)]

Heat No.	Aim Boron, %	Bar No.	Condition	Load, psi	Life, hr	Elong., %	Red. of Area, %	Min. 2nd Stage Creep Rate, %/hr
R394	0.1	2	As-Cast	8,000	5.0	43.0	74.0	3.8
		5	2150°F*24 hr	8,000	8.2	53.0	93.0	1.3
R419	0.1	1	As-Cast	7,000	14.4	26.0	71.5	0.80
		5	2150°F-1 hr	7,000	16.6	27.0	39.5	0.53
R435	0.1	1	As-Cast	6,500	57.8	64.0	72.5	0.45
		5	2150°F-24 hr	6,500	53.4	46.0	74.0	0.34
R344	0.5	3	As-Cast	8,500	17.0	25.5	65.0	0.96
		7	2150°F-24 hr	8,500	382	24.0	42.0	0.015
R396	0.5	2	As-Cast	8,500	108	23.0	49.5	No 2nd stage
		3	2150°F-1 hr	8,500	142	33.0	48.0	0.10
		5	2150°F-24 hr	8,500	445	18.0	50.5	0.008
R395	1.0	1	As-Cast	12,000	17.8	32.0	41.5	0.76
		2	2150°F-1 hr	12,000	26.5	38.0	41.5	0.47 (est.)
		3	2150°F-24 hr	12,000	48.7	39.0	50.0	0.29

*2150°F = 1177°C

TABLE VII

CREEP AND STRESS-RUPTURE PROPERTIES OF TEST BARS FROM HEAT R435, 0.10% B AIM ANALYSIS

(All tests conducted at 1500°F (816°C), 6500-psi load)

Bar No.	Pre-stress	Heat Treatment after Pre-stress	Life, hr	Elong., %	Red. of Area, %	Min. 2nd Stage Creep Rate, %/hr	Ratio Red. Area / Elong.
1	None	None	57.8	64.0	72.5	.45	1.13
6	0.4%	None	282	39.0	35.5	.061	.91
3	1.2%	None	237	42.0	47.5	.111	1.13
5	None	2150°F*-24 hr	53.4	46.0	74.0	.34	1.61
2	0.4%	2150°F -24 hr	145	44.0	53.0	.116	1.20
7	1.2%	2150°F -24 hr	65.9	41.0	62.5	.23	1.52

*2150°F = 1177°C

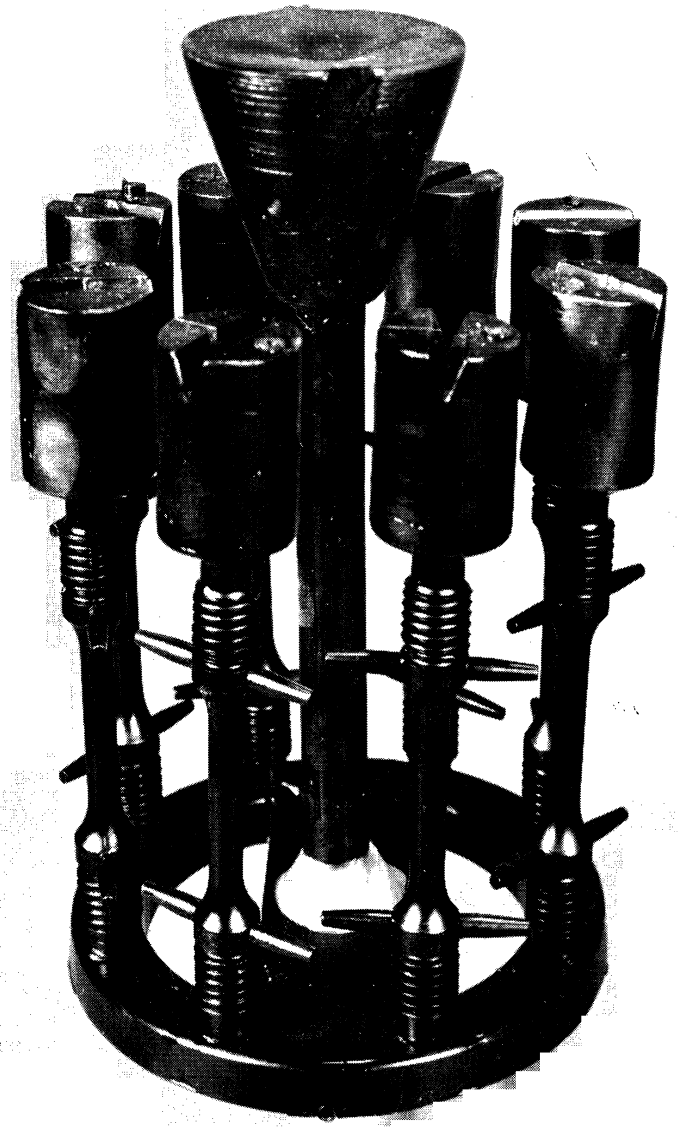

Figure 1. Photograph of a Pattern of Wax Tensile Specimens Illustrating the Gating System Used.

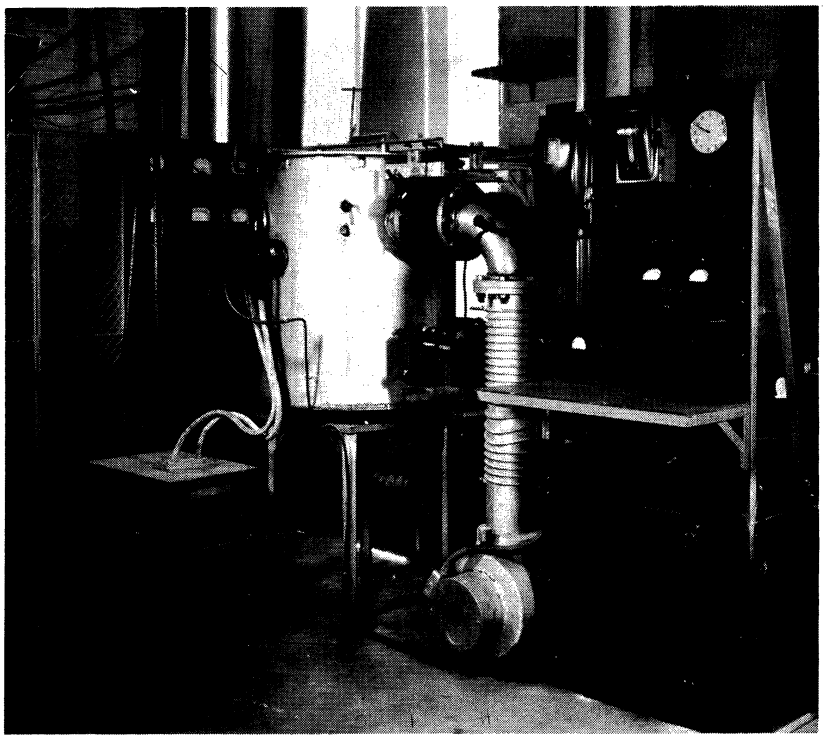

Figure 2. Photograph of Vacuum Induction Melting Equipment Showing Control Panels, Melting Shell, and Vacuum Pumps.

Figure 3. Interior of Vacuum Shell Showing the Induction Furnace, Mold, Charging Buckets, and Dipper.

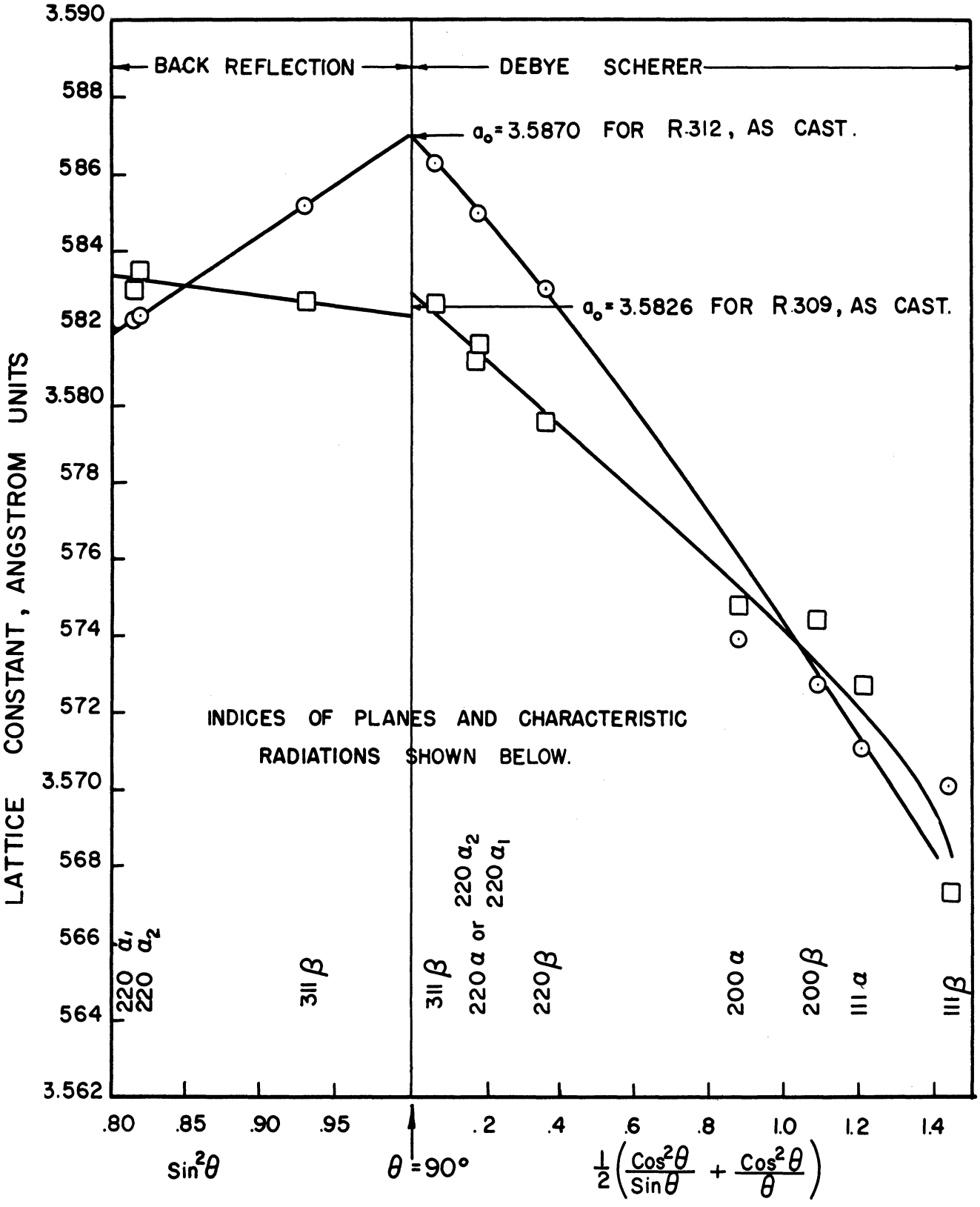

Figure 4. Typical Extrapolation Curves Used for the Precision Determination of the Lattice Parameter of Austenite.

1868-01*

A. R311, 0.10% B, 4.36% Boride By Volume. Austenite Hardness, 137.3 kg/mm^2.

1926-01

B. R312, 0.32% B, 9.92% Boride By Volume. Austenite Hardness, 139.5 kg/mm^2.

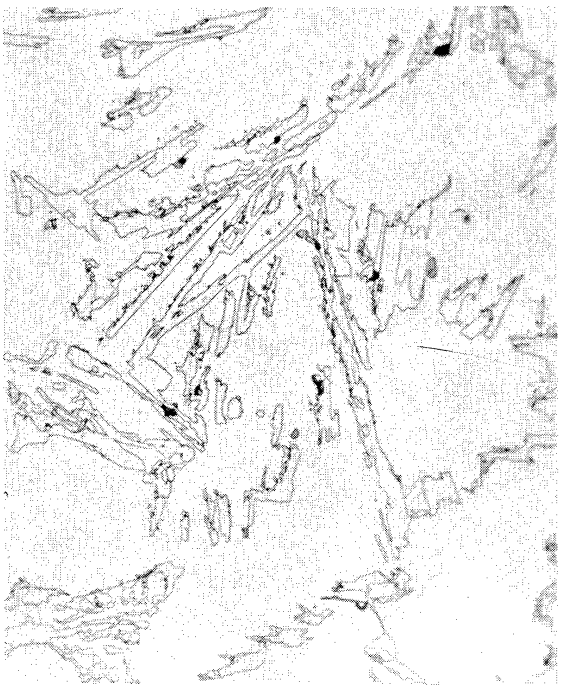

1836-01

C. R308, 0.80% B, 23.32% Boride By Volume. Austenite Hardness, 147.6 kg/mm^2.

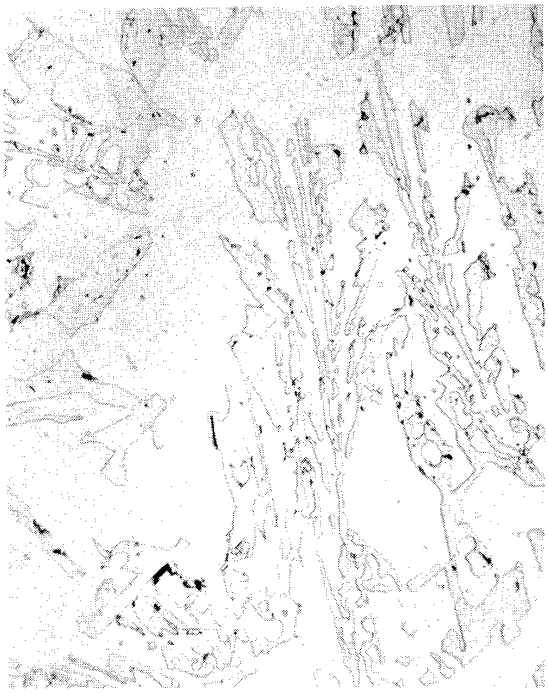

1870-04

D. R309, 1.49% B, 34.74% Boride By Volume. Austenite Hardness, 155.2 kg/mm^2.

Figure 5. Microstructure of As-Cast Alloys With Different Boron Contents. Magnification 500x.

*Numbers at the lower right-hand corner of all photomicrographs are identification numbers.

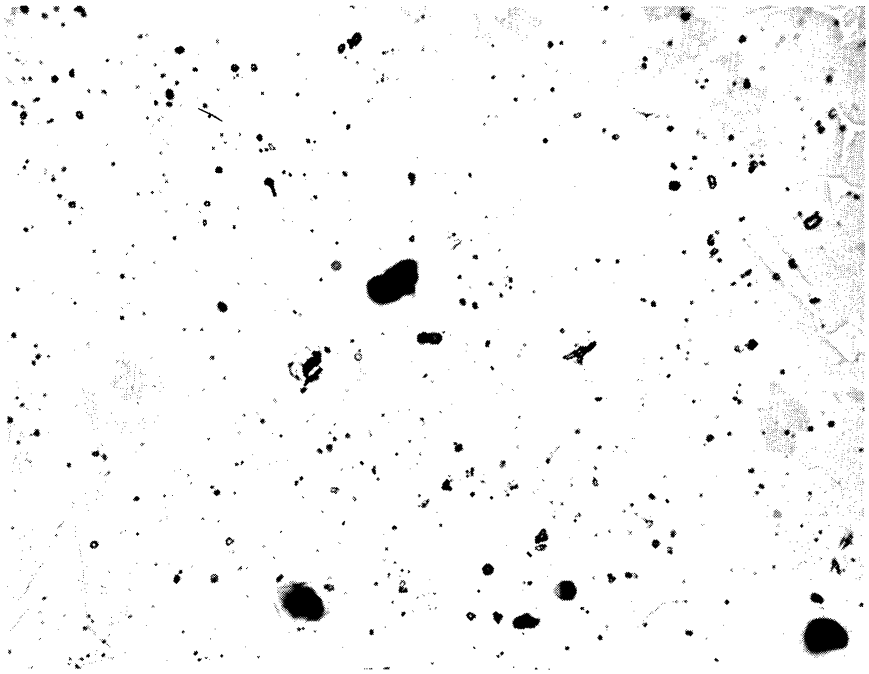

2246-01

Figure 6. Microstructure of Heat R371 Made to Aim Analyses FeCrB. Magnification 500x.

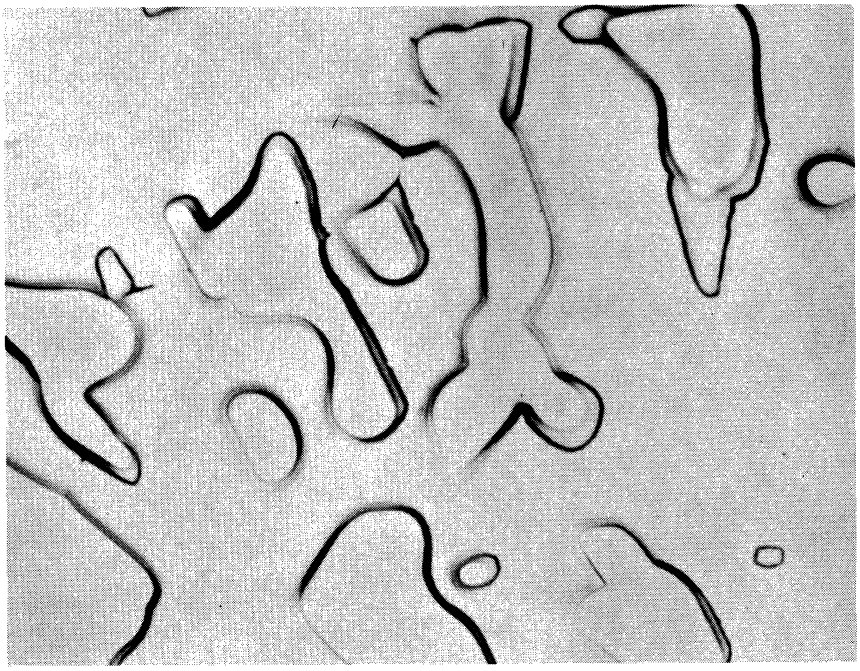

1973-01

Figure 7. Microstructure of Borides in Heat R309 at High Magnification After Severe Etching. Magnification 2000x.

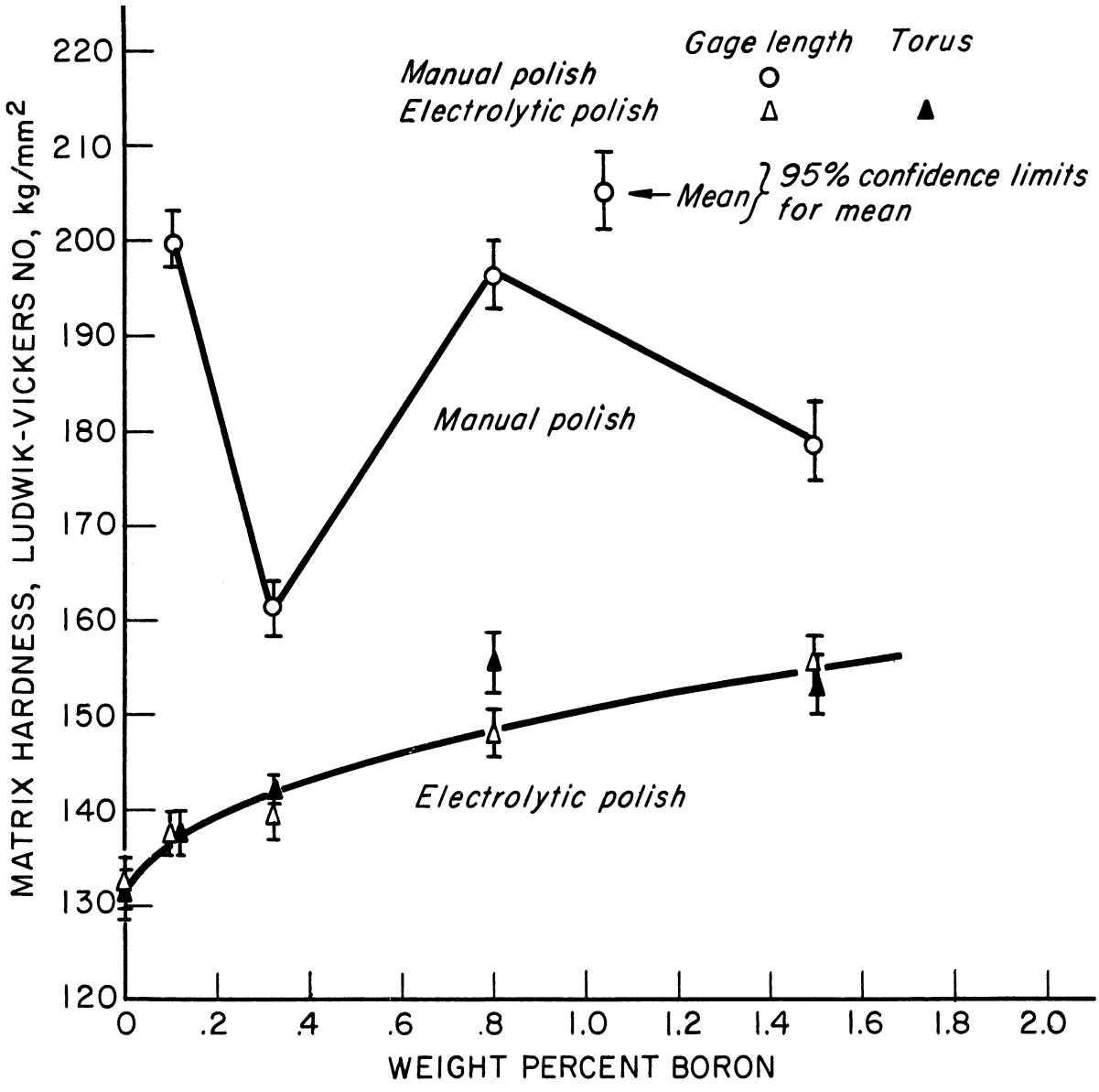

Figure 8. Microhardness of Austenite as a Function of Boron Content.

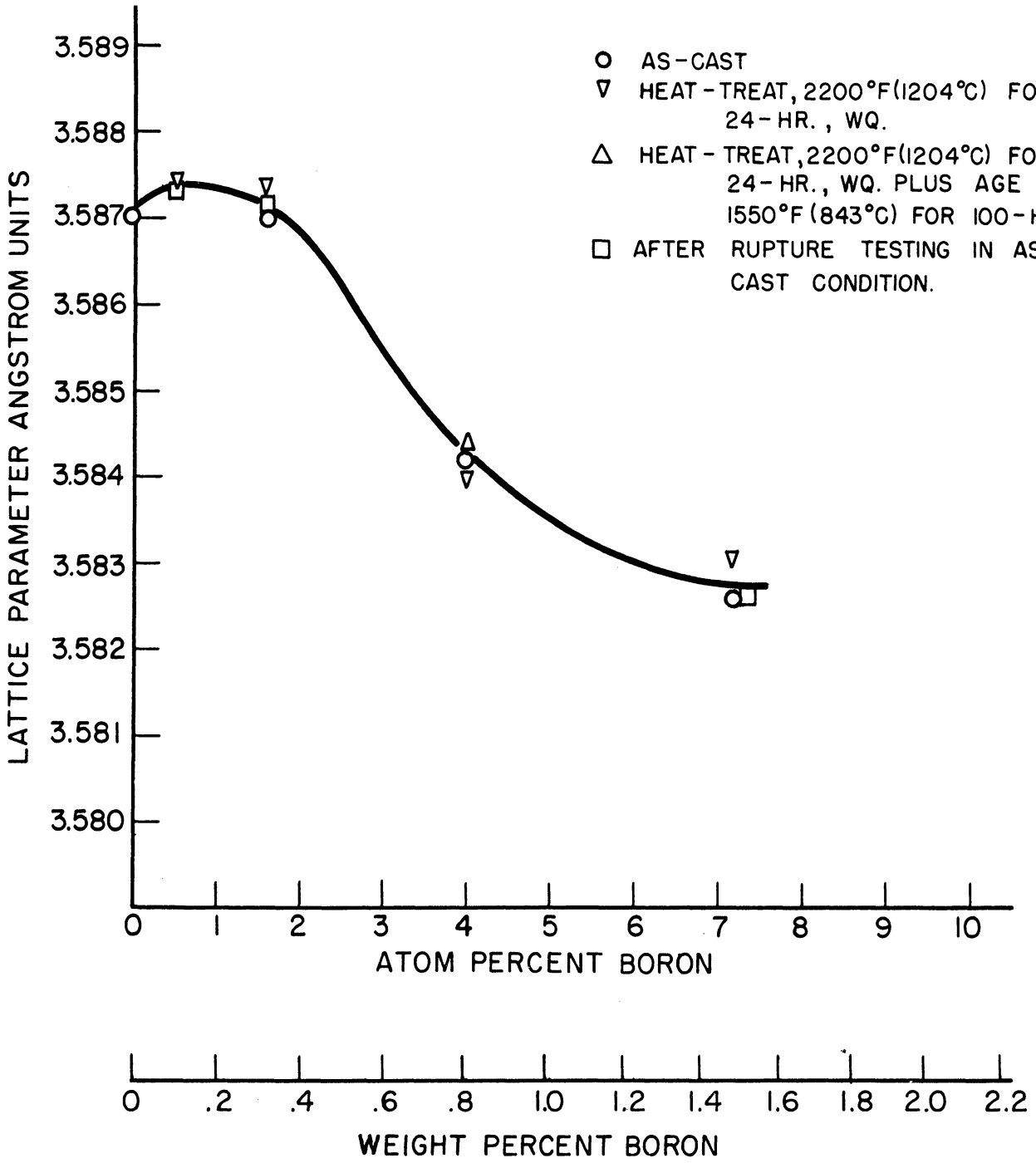

Figure 9. Lattice Parameter of Austenite in Heats R308 to R312 Obtained by Annealing Filings from Solid Samples. (Sample Preparation Method No. 1).

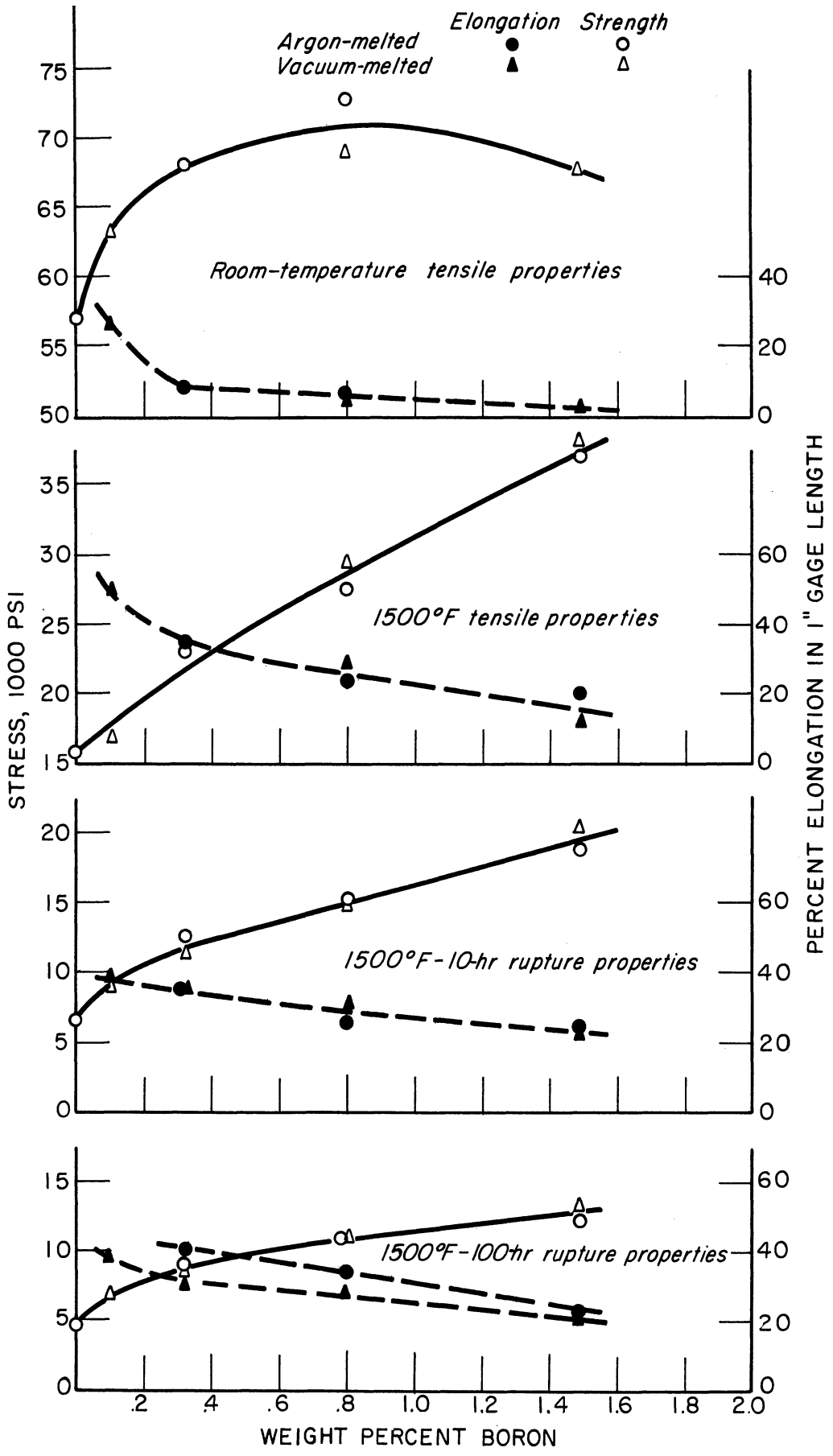

Figure 10. Mechanical Properties of 18.5% Ni, 20% Cr Austenite As a Function of Percent Boron.

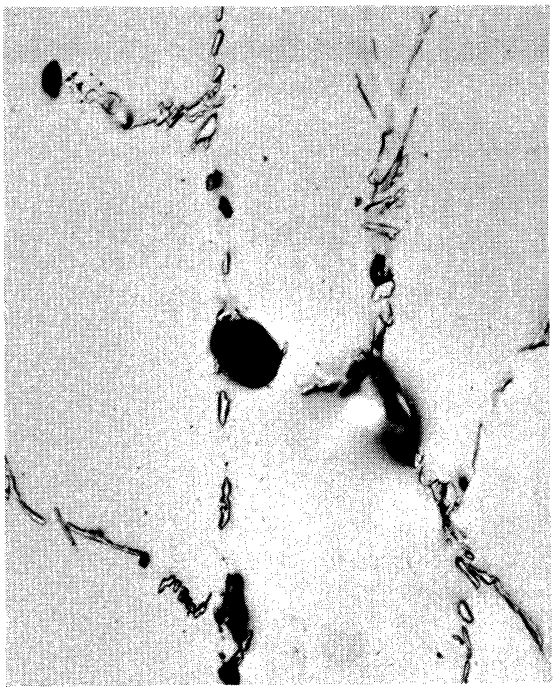

2194-02

A. R311-5, 0.10% B. 6000 psi Load, 400-hr. Life. Austenite Hardness, 128.5 kg/mm^2.

2196-01

B. R312-8, 0.32% B. 6800 psi Load, 166-hr. Life. Austenite Hardness, 132.0 kg/mm^2.

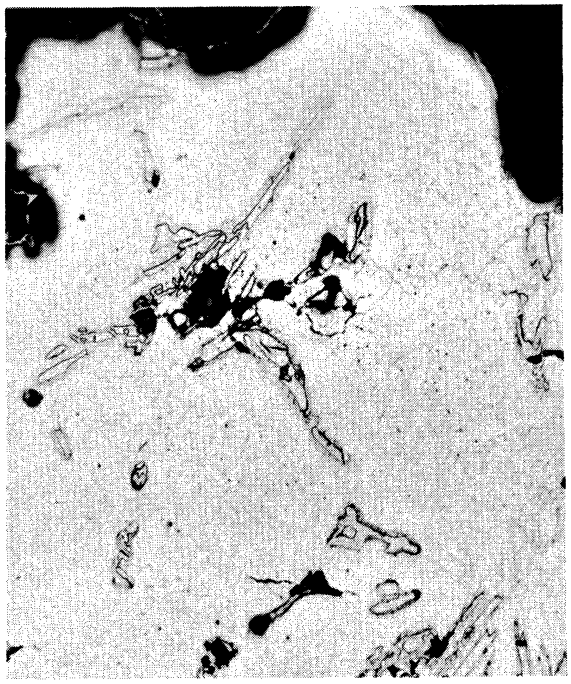

2199-01

C. R308-6, 0.80% B. 10,000 psi Load, 175-hr. Life. Austenite Hardness, 152 kg/mm^2.

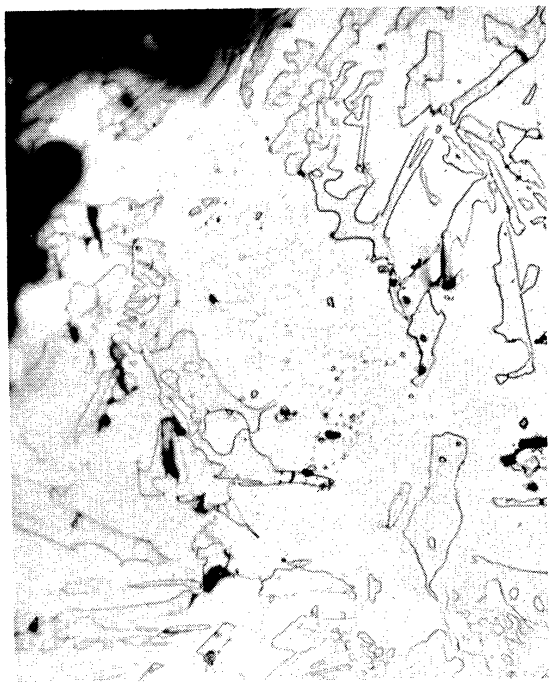

2191-01

D. R309-3, 1.49% B. 13,000 psi Load, 112-hr. Life. Austenite Hardness, 160.0 kg/mm^2.

Figure 11. Photomicrographs of Fractured Stress-Rupture Specimens Which Were Tested in the As-Cast Condition at 1500°F (816°C). Tensile Direction is Vertical in all Photomicrographs. Magnification 500x.

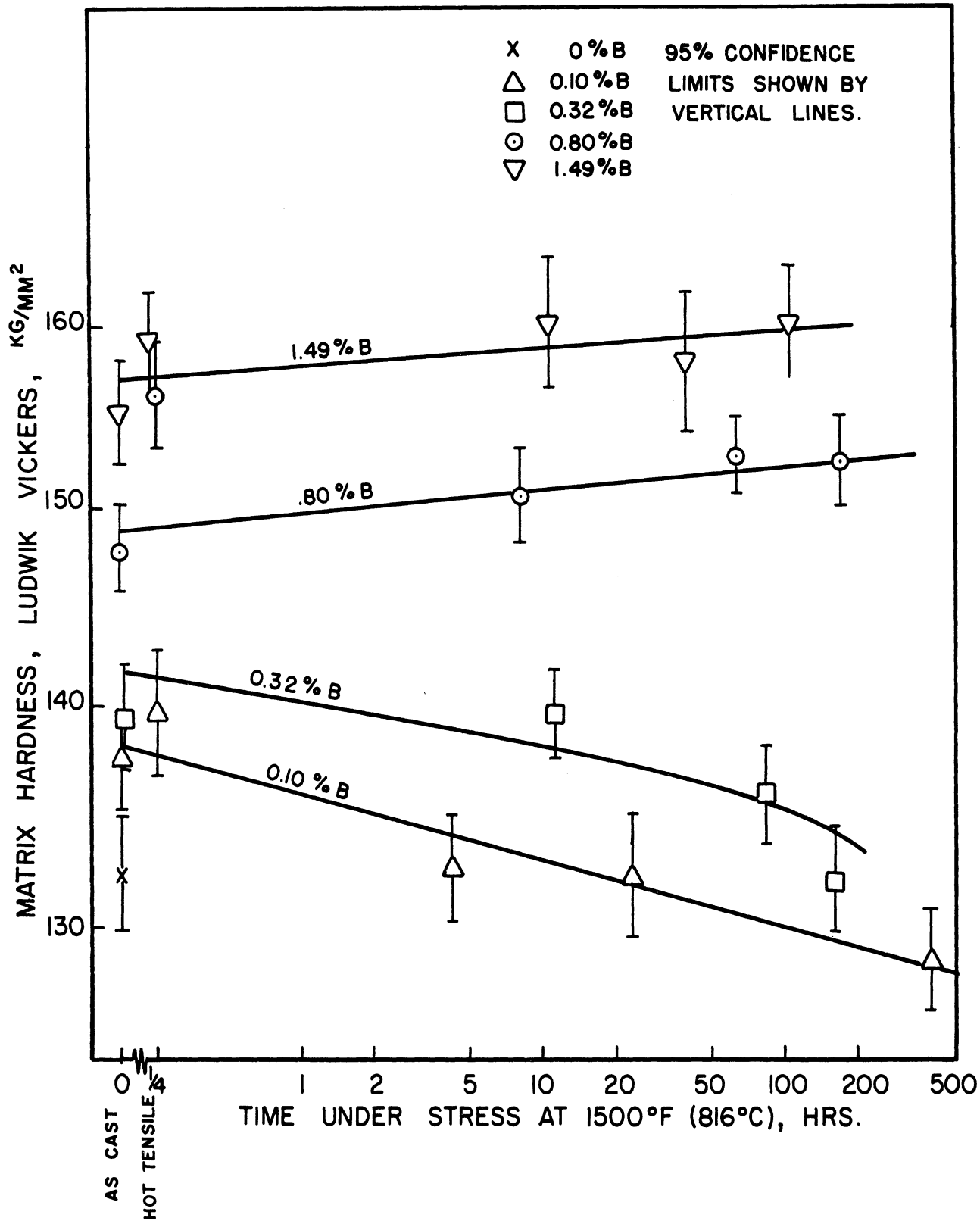

Figure 12. Microhardness of Austenite in Fractured Stress-Rupture Specimens Which Were Tested in the As-Cast Condition.

1972-01

A. R311, 0.10% B, Austenite
Hardness, 129 kg/mm^2.

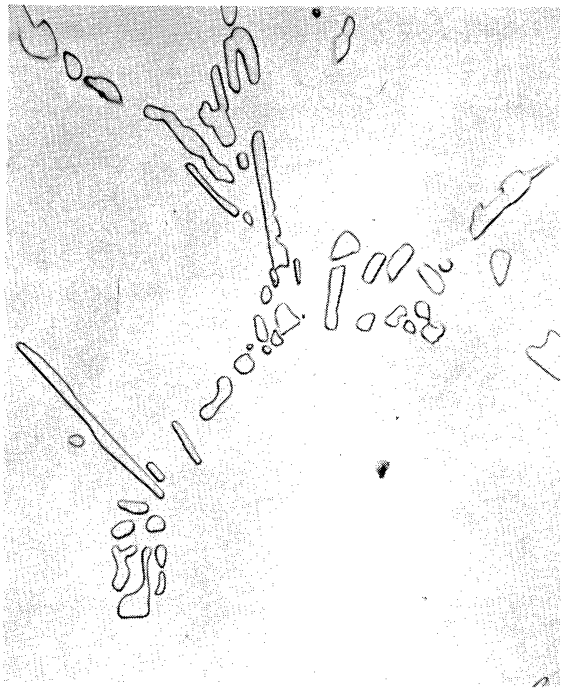

1966-01

B. R312, 0.32% B, Austenite
Hardness, 131 kg/mm^2.

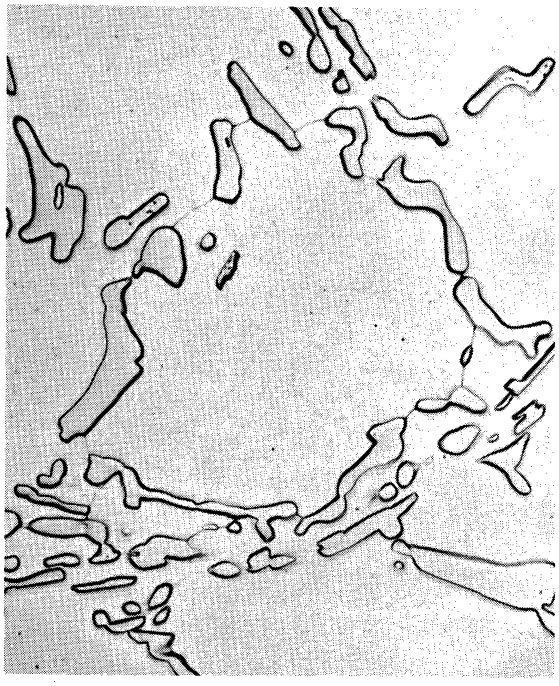

1974-02

C. R308, 0.80% B, Austenite
Hardness, 132 kg/mm^2.

1973-02

D. R309, 1.49% B, Austenite
Hardness, 129 kg/mm^2.

Figure 13. Microstructure of Alloys Heat-Treated at 2200°F(1204°C) for 24-hr. and Air-Quenched. Magnification 500x.

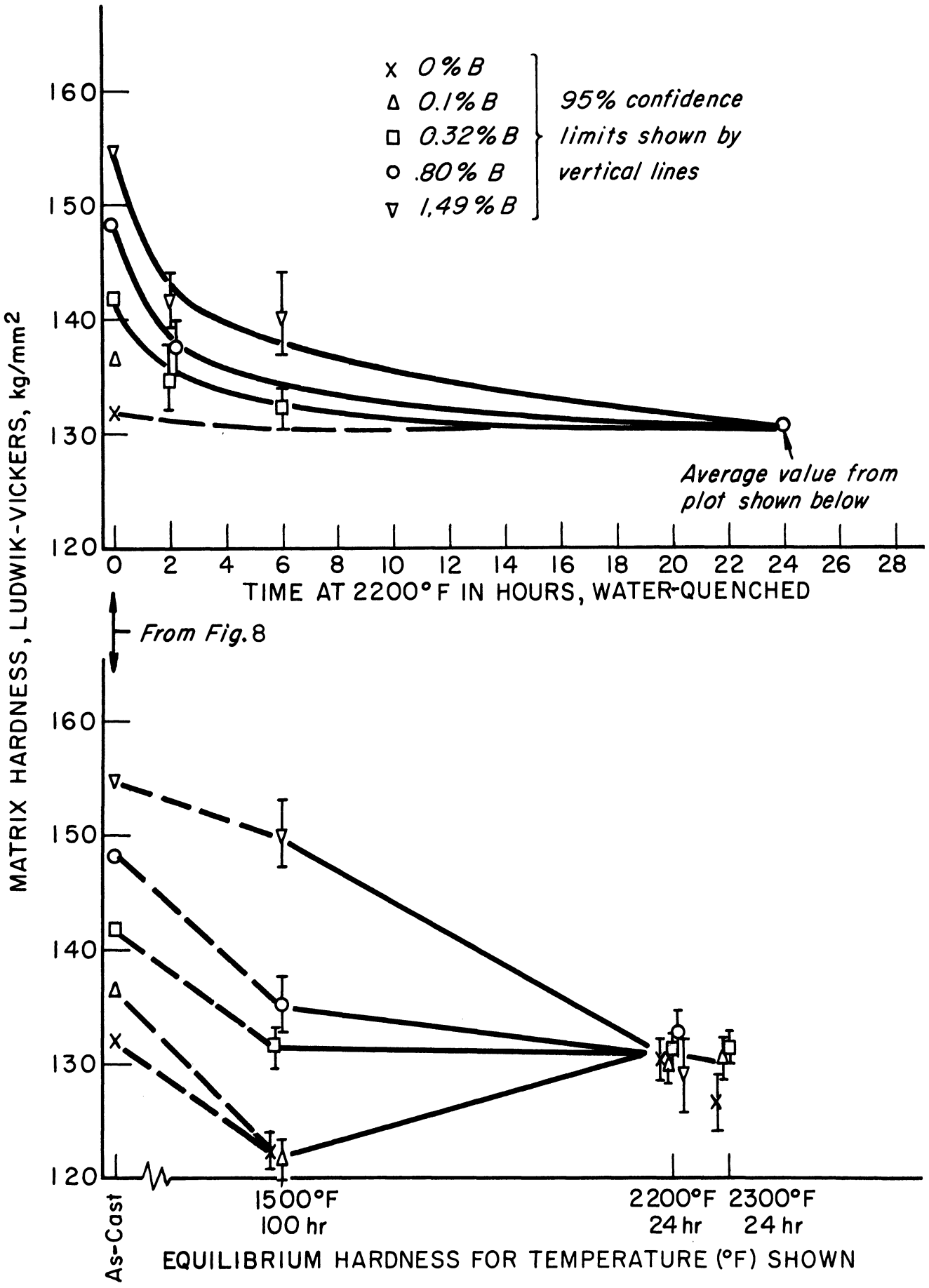

Figure 14. Microhardness of Austenite of Five Initial Heats After Heat Treatment.

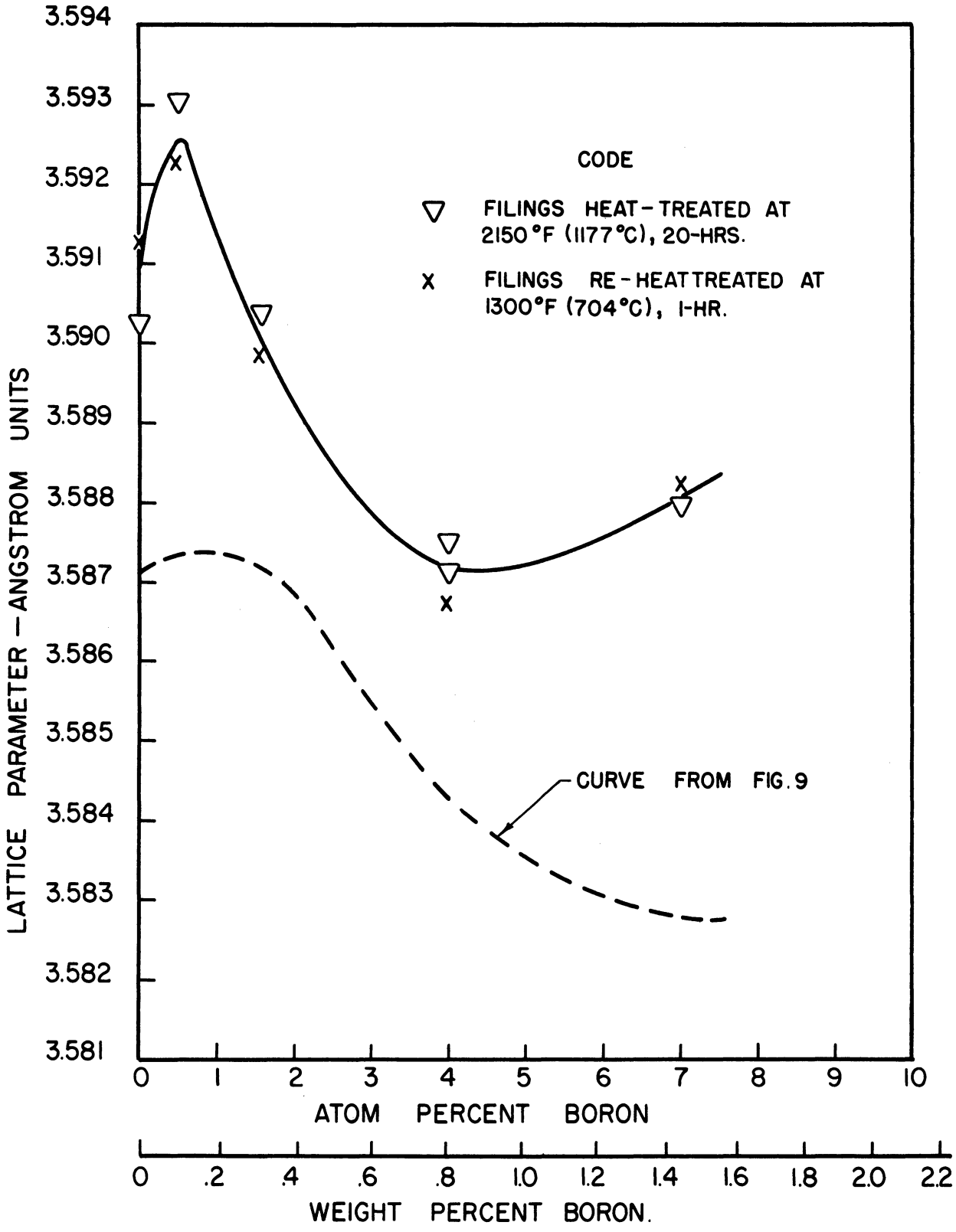

Figure 15. Lattice Parameter of Austenite in Heats R308 to R312 Obtained on Filings Which Had Been Given a High-Temperature Heat Treatment. (Sample Preparation Method No. 2).

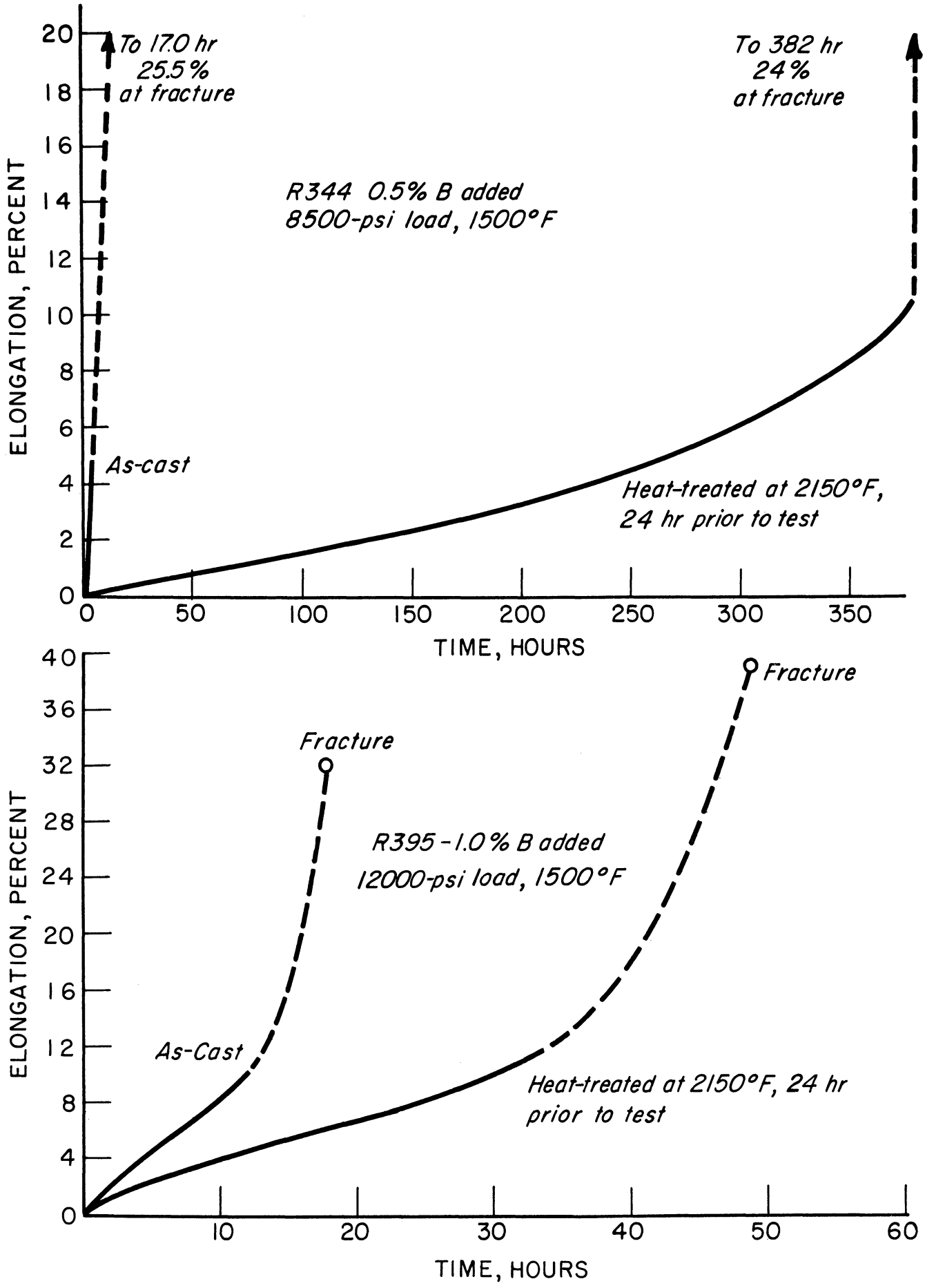

Figure 16. Typical Time Vs. Elongation Curves for Two Alloys Illustrating Effect of 2150°F (1177°C) Heat Treatment.

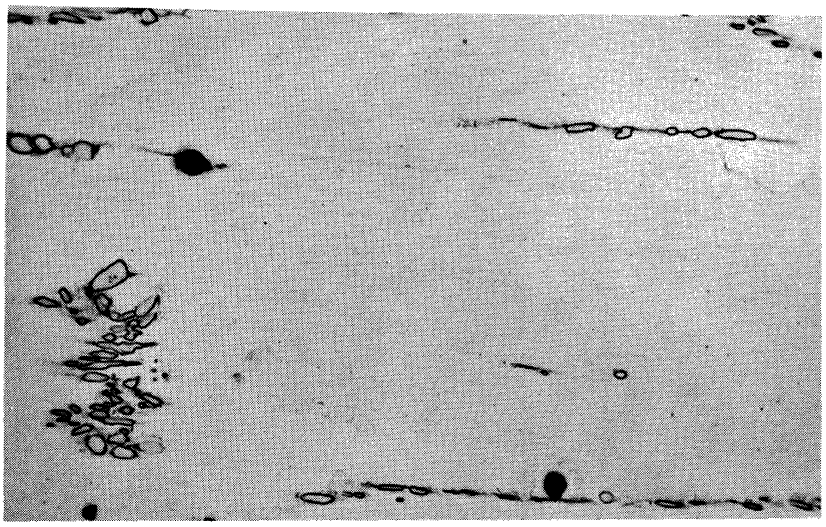

2455-01

A. R435-5, 0.10% B Aim Analysis. 6500 psi Load, 53.4-hr. Life.

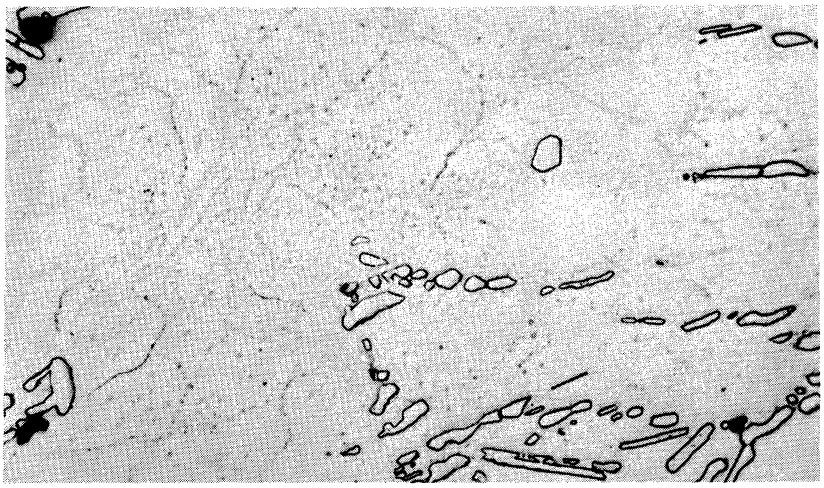

2323-01

B. R344-7, 0.50% B Aim Analysis. 8500 psi Load, 382-hr. Life.

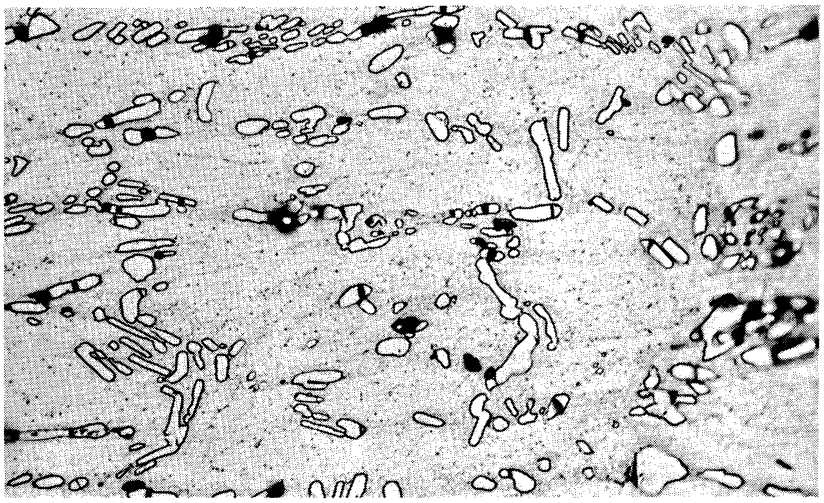

2375-01

C. R395-3, 1.0% B Aim Analysis. 12,000 psi Load, 48.7-hr. Life.

Figure 17. Microstructure of Fractured Stress-Rupture Specimens Which Were Tested Subsequent to Heat Treatment at 2150°F(1177°C) for 24-hrs. Tensile Direction is horizontal. Magnification 500x.

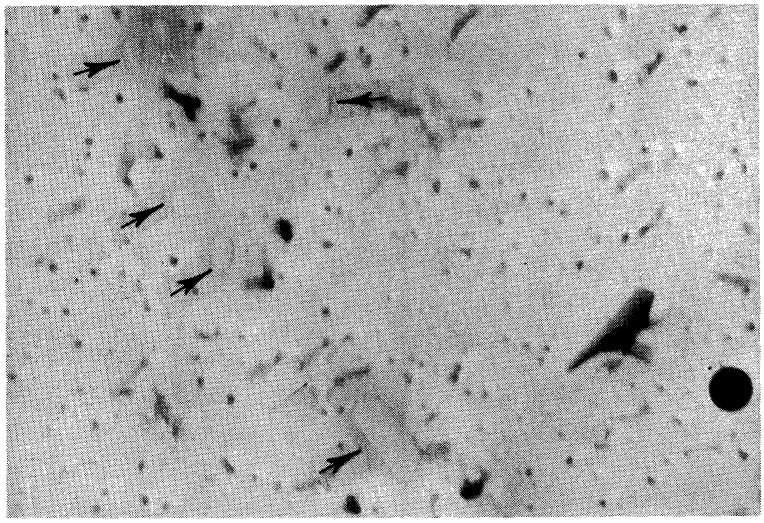

2323-E-02

Precipitate particles at subgrain boundaries are indicated by the arrows.

Figure 18. Electron Micrograph of Subgrain Boundary Precipitate Particles in Stress-Rupture Specimen R344-7 (see Figure 17 B). Magnification 18,000x.

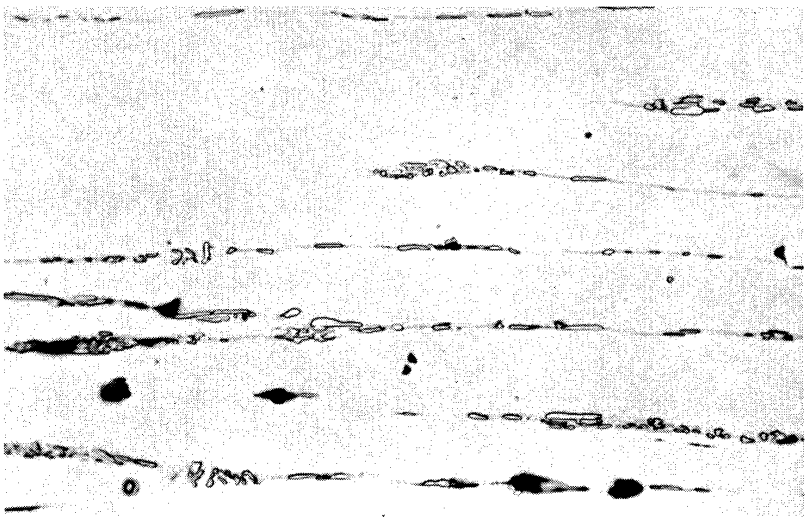

2452-01

A. R435-1, 0.10% B Aim Analysis, 6500 psi Load, 57.8-hr. Life.

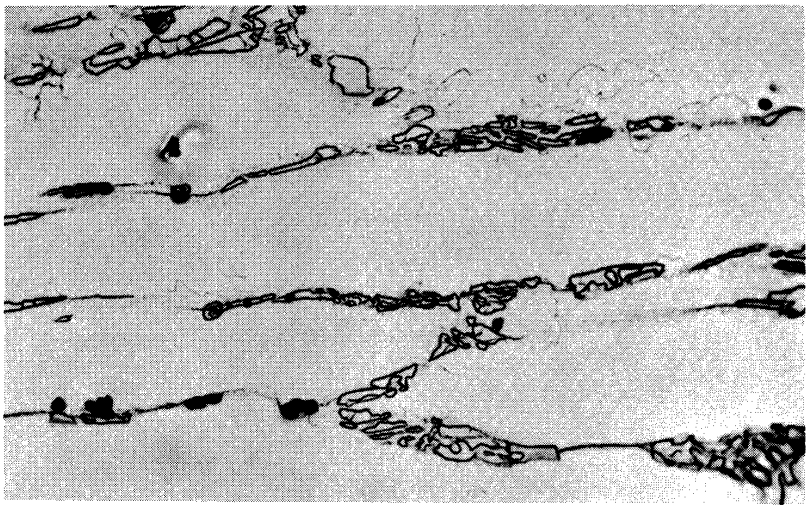

2373-01

B. R344-3, 0.50% B Aim Analysis, 8500 psi Load, 17.0-hr. Life.

2374-01

C. R395-1, 1.0% B Aim Analysis, 12,000 psi Load, 17.8-hr. Life.

Figure 19. Microstructure of Fractured Stress-Rupture Specimens from Same Heats as Shown in Figure 17, but from Bars Which Were Tested in the As-Cast Condition. Tensile Direction is Horizontal. Magnification 500x.

2251-03

A. Center Zone

Average diameter of this zone was .163-in. The hole into which the boron was packed was 1/16 or .063-in.diameter.

2251-02

B. Intermediate Zone

On the average, this zone had an inner diameter of .163-in. and an outer diameter of .219-in.

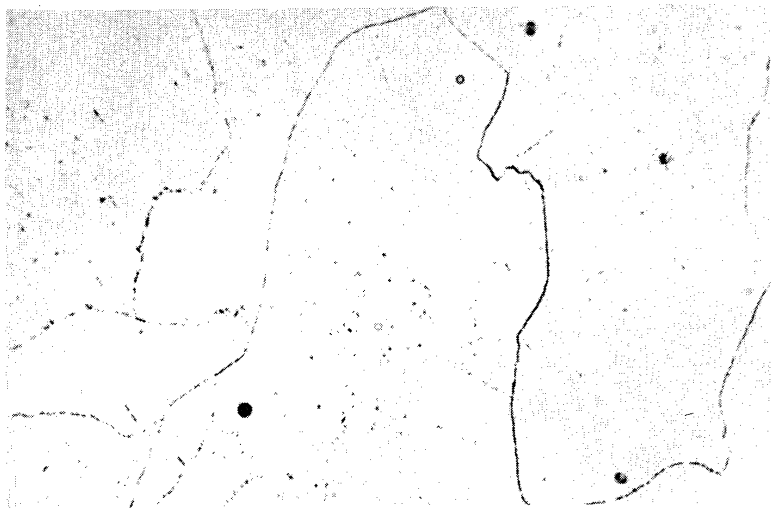

2251-01

C. Outer Zone

This zone extended from the termination of Zone B to the outside of the specimen which was .450-in. diameter.

Figure 20. Photomicrographs of Three Zones Produced in Diffusion Specimens. Magnification 500x.

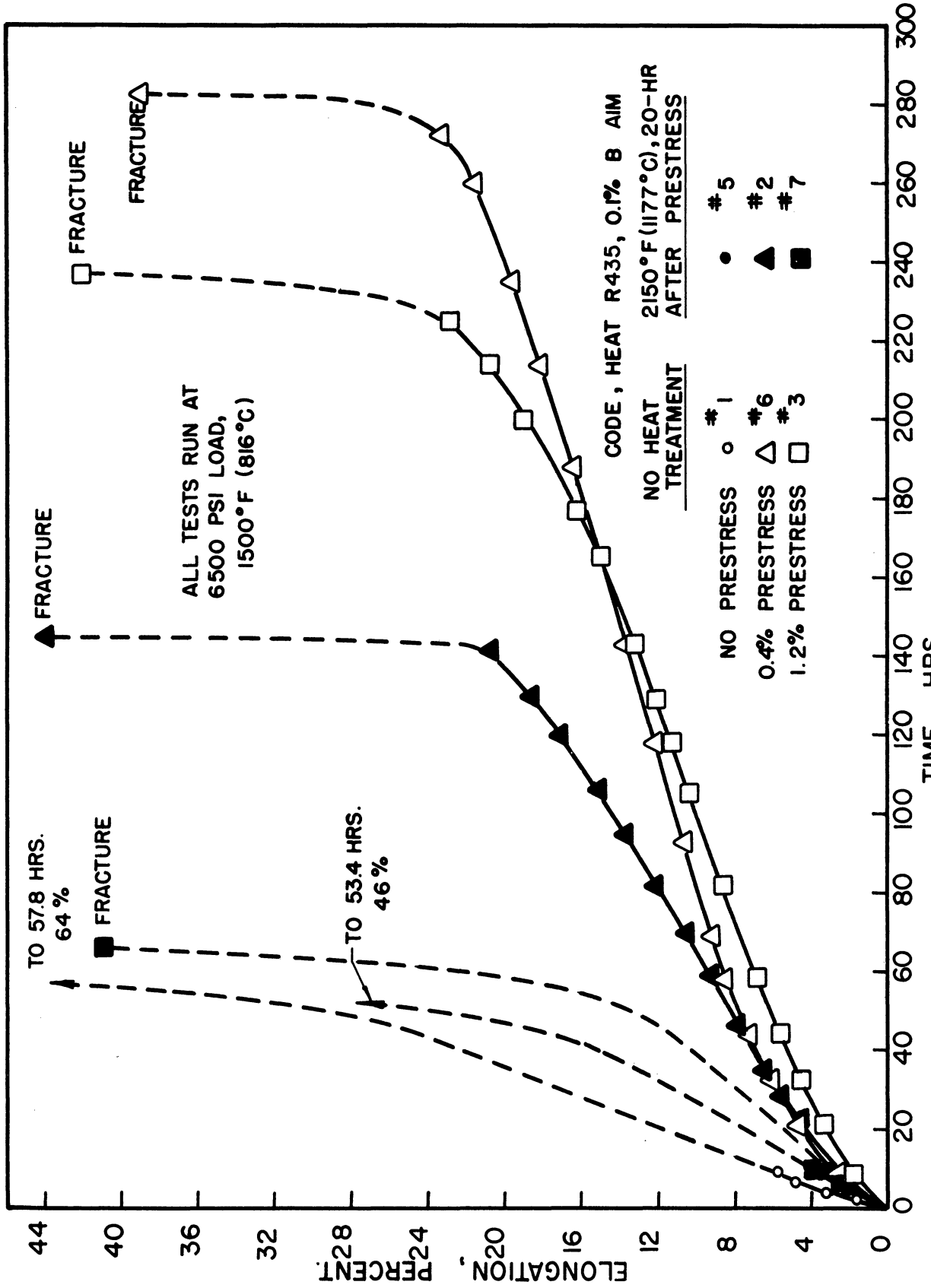

Figure 21. Creep-Rupture Curves Illustrating Effect of Prestressing on Heat R435.

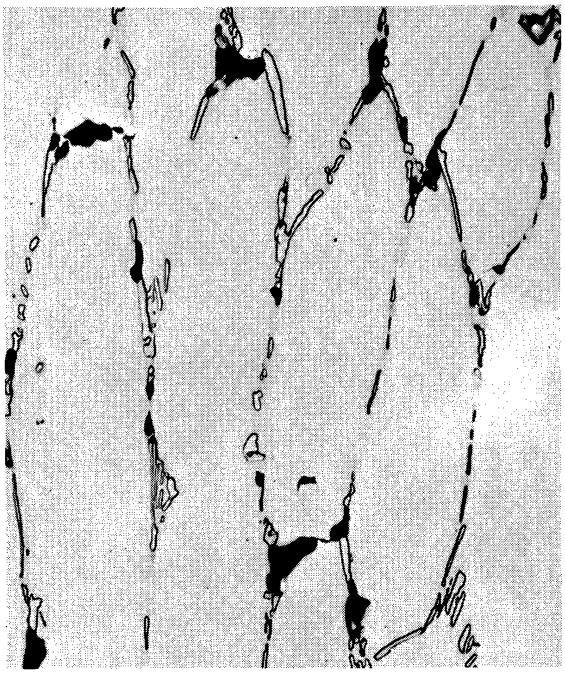

2461-01

A. Bar 6 - 0.4% Prestress, No Heat Treatment.

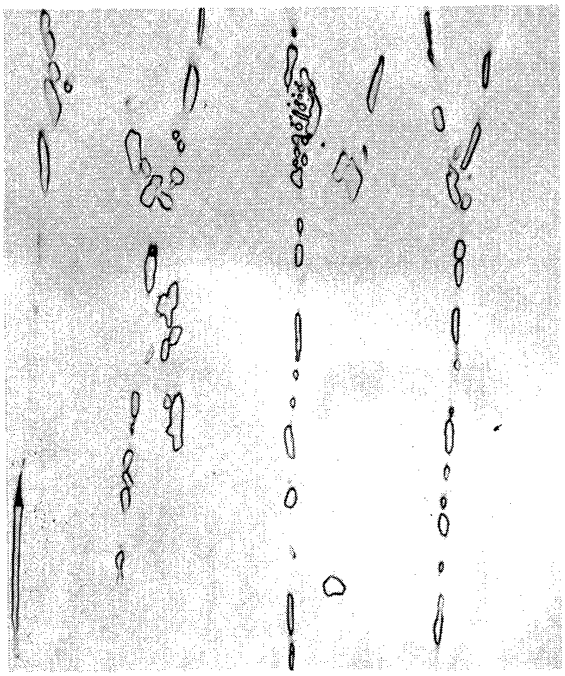

2453-01

B. Bar 2 - 0.4% Prestress, 2150°F(1177°C) 20-hr. Heat Treatment After Prestress.

2454-01

C. Bar 3 - 1.2% Prestress, No Heat Treatment.

2456-01

D. Bar 7 - 1.2% Prestress, 2150°F(1177°C) 20-hr. Heat Treatment After Prestress.

Figure 22. Microstructure of Fractured Rupture Specimens from Heat R435 Which were Prestressed Prior to Rupture Testing. All Specimens Tested at 6500 psi Load, 1500°F(816°C). Magnification 500x.

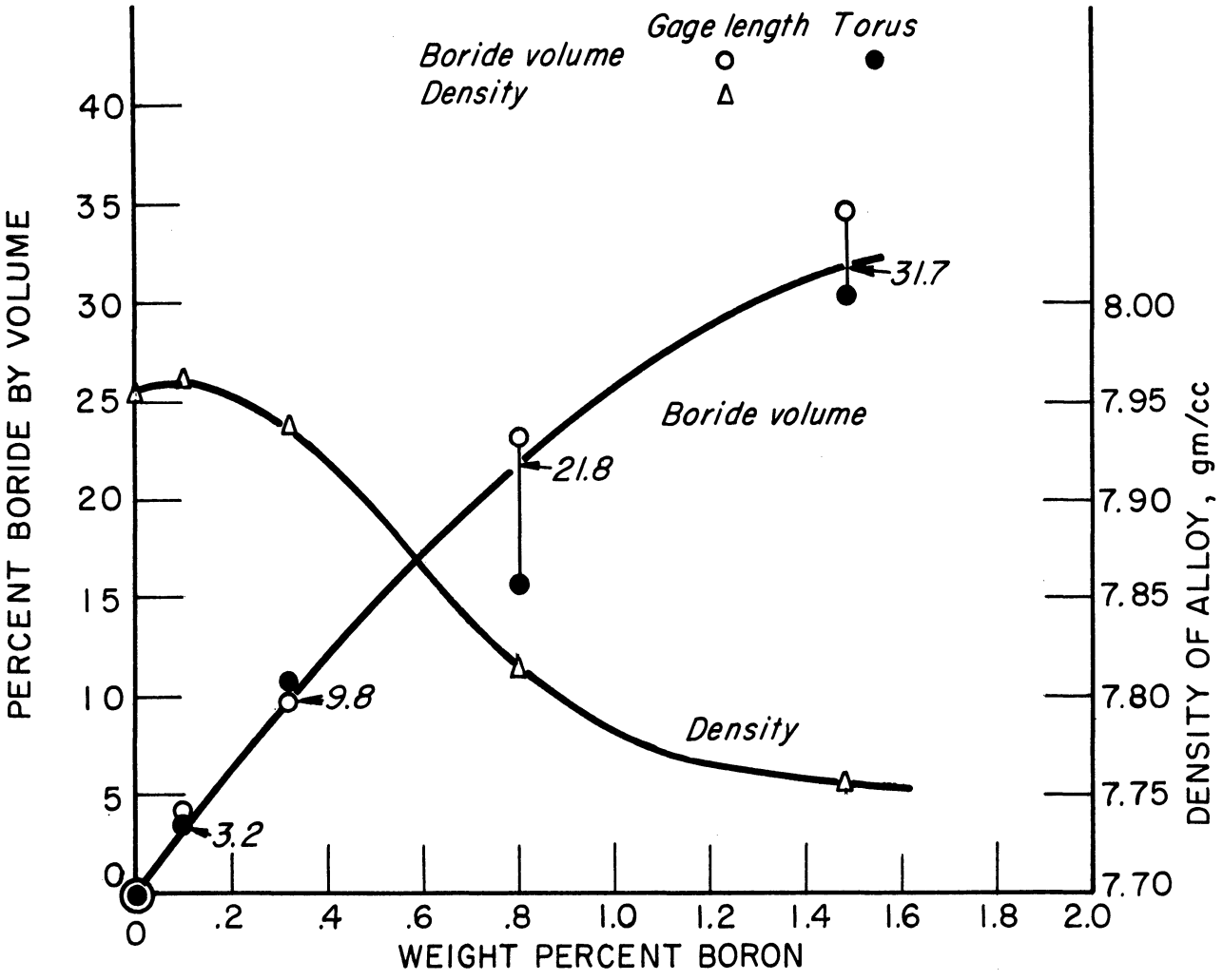

Figure 23. Relation Between Density, Boride Volume, and Boron Content of Five Initial Heats.

APPENDIX I

Sample Calculation of Microhardness and Computation of 95% Confidence Limits for Mean Value

Calculation of Microhardness

General: The superficial area (M) of a square pyramid with a known apex angle (α) and a known diagonal (d) of the base is given by:

$$M = \frac{d^2}{2 \sin \alpha/2} \quad .$$

For the pyramid of the Ludwik-Vickers diamond, $\alpha = 136°$, the value of the superficial area of the indentation is given by:

$$M = \frac{d^2}{2 \sin 68°} = \frac{d^2}{1.8544} \quad .$$

The value of the Ludwik-Vickers Hardness, load P per unit area M, is then given by:

$$H_V = \frac{P}{M} = 1.8544 \frac{P}{d^2} \text{ kg/mm}^2 \quad .$$

Specific: For the instrument at The University of Michigan, the calibration constant, m, between scale divisions, q, and diagonal length, d, has been evaluated. It is:

$$m = \frac{d}{q} = .1651 \frac{\text{microns}}{\text{divisions}} = 1.651(10)^{-4} \frac{\text{mm}}{\text{div}} \quad .$$

Therefore

$$H_V = \left[6.80(10)^4 \frac{P}{q^2}\right] \frac{\text{kg}}{\text{mm}^2} \text{ when } \begin{matrix} P \text{ is measured in gm} \\ q \text{ is measured in divisions} \end{matrix}$$

Example: Load = 18.3 gm, diagonal measured as 90 divisions

$$H_V = \frac{6.80(10)^4 \times 18.3}{90^2} = 154 \text{ kg/mm}^2 \quad .$$

Computation of 95% Confidence Limits for Mean Value

General: The method used involved computation of confidence intervals for the population mean when σ' was unknown. Therefore Student's t distribution was used (see Duncan,[39] pages 345-346). This computation was made for the 25-scale readings (the q values). The mean hardness and 95% confidence limits for the mean hardness were then computed at the end.

Example: R311, 0.10% B heat, microspecimen from gage length of tensile bar, as-cast, microspecimen no. 1868.

1. Computation of mean and standard deviation.

q	Frequency f	u	fu	fu^2
92	1	-3	-3	9
93	5	-2	-10	20
94	4	-1	-4	4
95	4	0	0	0
96	5	1	5	5
97	3	2	6	12
98	2	3	6	18
99	0	4	0	
100	1	5	5	25
	N = 25		Σu 5	Σu^2 93

$\bar{q} = 95 + 5/25 = 95.20$

$\sigma_q = 1/N \sqrt{N \Sigma u^2 - (\Sigma u)^2} = 1/25 \sqrt{25 \times 93 - 5^2} = 1.92$

$s_q = \sigma_q \sqrt{N/N-1} = 1.92 \sqrt{25/24} = 1.96$

2. Computation of 95% confidence limits for mean of q values.

95% C.L. given by $\bar{q} \pm \frac{t_{0.025}\, s_q}{\sqrt{N}}$ where $t_{0.025} = 2.064$ for a sample size of 25 ($t_{0.05}$ for two tail areas and n = N-1 = 24)

95% C.L. for $\bar{q} = 95.20 \pm \frac{2.064 \times 1.96}{\sqrt{25}} = 95.20 \pm .81$

3. Computation of 95% confidence limits of microhardness.

$$\text{Lower 95\% C.L.} = \frac{6.80(10)^4 \times 18.3}{(94.39)^2} = 135.0 \text{ kg/mm}^2$$

$$\text{Mean} = \frac{6.80(10)^4 \times 18.3}{(95.20)^2} = 137.3 \text{ kg/mm}^2$$

$$\text{Upper 95\% C.L.} = \frac{6.80(10)^4 \times 18.3}{(96.01)^2} = 139.8 \text{ kg/mm}^2$$

APPENDIX II

Material Balance and Calculation of Lattice Parameter of Austenite Based upon Vegard's Law for Heat R309

Material Balance, R309

1. 100 cc of R309 will consist of approximately 31.7 cc of boride and 68.3 cc of austenite (Fig. 23). This volume of boride weighs 31.7 x 5.255 = 166.6 gm.

2. The boride analysis reported was probably in error. It was assumed that all the boron present in the heat was in the boride and that the error in analysis on the other three elements, Ni, Cr, Fe, was proportional to the amount of each found by actual analysis.

a. 100 cc of heat R309 weighs 100 x 7.755 = 775.5 gm

b. weight of boron in 100 cc of alloy = 1.49% of 775.5 gm = 11.55 gm

c. computation of weight of alloy in boride.

				Corrected Wt.	Corrected %	Analyzed %
Ni	1.90% x 166.6 gm	=	3.17 gm	3.95	2.37	1.90
Cr	25.27% x 166.6	=	42.10	52.40	31.45	25.27
Fe	47.6 % x 166.6	=	79.30	98.70	59.24	47.6
B	From step b	=	11.55	11.55	6.94	13.84
			136.12 gm	166.60	100.00	88.61

3. The Ni, Cr, and Fe content of the austenite therefore is found as follows.

	% in alloy		Wt. 100 cc		Gm in alloy		Gm in boride		Gm in austenite	% in austenite
Ni	18.7	x	775.5 gm	=	145.02	-	3.95	=	141.07	23.2
Cr	19.0	x	775.5	=	147.35	-	52.40	=	94.95	15.6
Fe	60.81*	x	775.5	=	471.58	-	98.70	=	372.88	61.2
B	1.49	x	775.5	=	11.55	-	11.55	≈	0.00	-
					775.50				608.90	100.0

*Iron analysis by difference

Calculation of Lattice Constant by Vegard's Law

To make this computation, the measured lattice constant and chemical analysis of the zero percent boron heat, R310, were used as a reference.

1. Austenite composition

	R310 (0% B)		R309 (1.49% B)	
	Wt. %	Atom. %	Wt. %	Atom. %
Ni	18.26	17.26	23.2	22.05
Cr	20.73	22.14	15.6	16.75
Fe	61.01*	60.60	61.2	61.20
		100.00		100.00

2. A weighted average of the atomic radii, in angstrom units, is computed as follows.

	R310		R309	
Ni	.1726 x 2.49 =	.430	.2205 x 2.49 =	.549
Cr	.2214 x 2.57 =	.569	.1675 x 2.57 =	.430
Fe	.6060 x 2.52 =	1.527	.6120 x 2.52 =	1.542
		2.526		2.521

3. The estimated lattice constant of R309 therefore is found from the relation:

$$a_o \text{ of } 0\% \text{ B heat} \times \frac{\text{Avg. atomic radius R309}}{\text{Avg. atomic radius R310}}$$

$$3.587 \times \frac{2.521}{2.526} = 3.580 \text{ angstrom units}$$

*Iron analysis by difference

REFERENCES

1. Grange, R. A., et al., "Boron, Calcium, Columbium and Zirconium in Iron and Steel," Alloys of Iron Monograph, John Wiley and Sons, Inc., New York, 1957.

2. Morgan, E. R., and Shyne, J. C., "Preparation and Properties of Boron Treated Nonaging Open Hearth Steels," Journal of Metals, 9 (1957), 781-785.

3. Kraft, R. W., and Flinn, R. A., Cast Iron-Base Heat-Resistant Alloys, Univ. of Mich. Eng. Res. Inst. Report 2313-7-P (Ann Arbor, August, 1957) and Report 2698-2-F (Ann Arbor, February, 1958) (both Confidential).

4. Wasmuht, R., "Über Härtungserscheinungen der Eisen-Bor-Legierungen unter besonderer Berücksichtigung der Ausscheidungshärtung," Arch. Eisenhüttenw., 5 (1931), 261-266. (Bruchter translation No. 1885.)

5. Bennek, H., and Schafmeister, P., "Ausscheidungshärtung der Stahle mit 18% Cr und 8% Ni durch Zusatz von Beryllium, Bor oder Titan und ihr Einfluss auf die Korrosionsbeständigkeit," Arch. Eisenhüttenw. 5 (1932), 615-620. (Bruchter translation No. 84.)

6. Cornelius, H., "Die Härtung borhaltiger austenitischer Chrom-Nickel-Stahle beim Anlassen," Arch. Eisenhüttenw., 12 (1939), 499-505. (Bruchter translation No. 979.)

7. Comstock, G. F., "A New Alloy Steel for High Temperature Use," Metal Progress, 56 (July, 1949), 67-71.

8. Miller, J., Smith, L. W., and Porter, P. K., Utilization of Low Alloy Materials for High Temperature Service Applications, U.S.A.F Air Materiel Command, AF Technical Report 5929, June, 1949.

9. Guy, A. G., "Nickel Base Alloys for High Temperature Applications," Trans. Am. Soc. for Metals, 41 (1949), 125-140.

10. Corey, C. L., and Freeman, J. W., Investigation of the Influence of Boron and Titanium on the High Temperature Properties of Cr-Ni-Mo-Fe Austenitic Alloys, Wright Air Development Center, WADC Technical Report 54-583, December, 1954.

REFERENCES (continued)

11. Blatz, W. E., Reynolds, E. E., and Dyrkacz, W. W., "Influence of Boron on Cast Cobalt Base S-816 Alloy," Symposium on Metallic Materials for Service at Temperatures Above 1600°F, Am. Soc. for Testing Mat., STP No. 174 (1956), 16-23.

12. Strauss, J., Discussion of paper by Blatz, Reynolds, and Dyrkacz, Symposium on Metallic Materials for Service at Temperatures Above 1600°F, Am. Soc. for Testing Mat., STP No. 174 (1956), 25-27.

13. Koffler, R. W., Pennington, W. J., and Richmond, F. M., The Effect of Small Amounts of Boron and Zirconium on the High Temperature Properties of Vacuum Melted Super Alloys, Universal Cyclops Steel Corp., Research and Development Department, Report No. 48, June 11, 1956.

14. Decker, R. F., Rowe, J. P., and Freeman, J. W., Influence of Crucible Materials on High-Temperature Properties of Vacuum Melted Nickel-Chromium-Cobalt Alloy, NACA TN 4049, 1957.

15. Pennington, W. J., "Improvement in High-Temperature Alloys by Boron and Zirconium," Metal Progress, 73 (March, 1958), 82-86.

16. Decker, R. F., The Mechanism of Beneficial Effects of Boron and Zirconium on Creep-Rupture Properties of a Complex Heat-Resistant Alloy, University of Michigan Doctoral Dissertation, 1957.

17. Grange, R. A., and Garvey, T. M., "Factors Affecting the Hardenability of Boron Treated Steels," Trans. Am. Soc. Metals, 37 (1946), 136-174.

18. Kreshchanovski, N. S., Prosvirin, V. I., and Ginzburg, E. S., "Effect of Boron on the Properties of Cast Austenitic Steel of the 15% Cr, 25% Ni type," Liteinoe Proizvodstvo, No. 5 (1954), 16-19.

19. Spretnak, J. W., and Speiser, R., "A Hypothesis for the Boron Hardenability Mechanism," Trans. Am. Soc. Metals, 46 (1954), 1089-1119.

20. Simcoe, C. R., Elsea, A. R., Manning, G. K., "Study of the Effect of Boron on the Decomposition of Austenite," Am. Inst. Mining and Met. Engineers, 203, Journal of Metals, 7 (1955), 193-200.

21. Spretnak, J. W., and Speiser, R., "Grain Boundary Films in Boron Steels," Am. Inst. Mining and Met. Engineers, 197, Journal of Metals, 5 (1953), 445-446.

REFERENCES (continued)

22. Goldhoff, R. M., and Spretnak, J. W., "Distribution of Boron in Gamma Iron Grains," Trans. Am. Inst. Mining and Met. Engineers, 209, Journal of Metals, 9 (October, 1957), 1278-1283.

23. Wever, F., and Muller, A., "Über die Zweistoffsysteme Eisen-Bor und Eisen-Beryllium mit einem Beitrag zur Kenntnis des Zweistoffsystems Eisen-Aluminum," Mitt. Kaiser-Wilhelm Inst. Eisenforsch., 11 (1929), 193-223.

24. McBride, C. C., Spretnak, J. W., and Speiser, R., "A Study of the Fe-Fe_2B System," Trans. Am. Soc. for Metals, 46 (1954), 499-520.

25. Nicholson, M. E., "Constitution of Fe-B Alloys in the Low Boron Range," Trans. Am. Inst. of Mining and Met. Engineers, 200, Journal of Metals, 6 (1954), 185-190.

26. Kiessling, R., "The Crystal Structure of Molybdenum and Tungsten Borides," Acta Chem. Scand., 1 (1947), 893-916.

27. Kiessling, R., "The Borides of Some Transition Elements," Acta Chem. Scand., 4 (1950), 209-227.

28. X-Ray Diffraction Card Data and Supplements, Am. Soc. for Testing Mat., Philadelphia, Pa.

29. Schwarzkopf, P., and Kieffer, R., Refractory Hard Metals—Borides, Carbides, Nitrides and Silicides, The MacMillan Co., New York, 1953.

30. Kiessling, R., "The Binary System Cr-B," Acta Chem. Scand., 3 (1949), 595-602.

31. Anderson, L. H., and Kiessling, R., "Investigations on the Binary Systems of B with Cr, Cb, Ni, and Ti Including a Discussion of the Phase TiB in the Ti-B System," Acta Chem. Scand., 4 (1950), 160-164.

32. Steinitz, R., private communication to the author.

33. Bjurstrom, T., Arkiv. Kemi Mineral. Geol. [A], 11 (1933), 5.

34. Rundqvist, S., "Two Borides with Cementite Structure," Nature, 181 (January 25, 1958), 259.

35. Halla, F., Kristallchemie und Kristallphysik metallischer Werkstoffe, Barth, Leipzig, 1939.

REFERENCES (concluded)

36. Post, B., Pipitz, C., and Herz, M., "A New Ternary Boride," Powder Met. Bull., 7 (April, 1956), 149-152.

37. Solomon, P., private communication to the author.

38. Gurry, R. W., "The Relative deoxidizing Power of Boron in Liquid Steel and the Elimination of Boron in the Open-Hearth Process," Trans. Am. Inst. Mining Met. Engineers, 158 (1944), 98-106.

39. Duncan, A. J., Quality Control and Industrial Statistics, Richard D. Irwin, Inc., Homewood, Illinois, 1953.

40. Klug, H. P., and Alexander, L. E., X-Ray Diffraction Procedures, John Wiley and Sons, Inc., New York, 1954.

41. Byrne, P.J.S., and Hansen, H. L., "Preparation of Powder Samples for Use in Focusing Cameras," Norelco Reporter, 3 (1956), 107.

42. Nelson, J. B., and Riley, D. P., "An Experimental Investigation of Extrapolation Methods in the Derivation of Accurate Unit Cell Dimensions of Crystals," Proc. Phys. Soc., 57 (1945), 160.

43. Mahla, E. H., and Nielsen, N. A., "Carbide Precipitation in Type 304 Stainless Steel," Trans. Am. Soc. Metals, 43 (1951), 290.

44. Wolszon, J. D., Hayes, J. R., and Hill, W. H., "Applications of Anion-Exchange Resins to Determination of Boron," Anal. Chem., 29 (1957), 829-832.

45. Wilcox, L. V., "Determination of Boron in Natural Waters and Plant Materials," Ind. Engrg. Chem., Anal. ed., 2 (1930), 358-361.

46. Cottrell, A. H., "Creep and Aging Effects in Solid Solutions," in Creep and Fracture of Metals at Elevated Temperatures, Her Majesty's Stationery Office, London, 1956, pp. 141-152.

47. Glen, J., "An Experimental Study of the Strength and Ductility of Steel at Elevated Temperatures," Symposium on Strength and Ductility of Metals at Elevated Temperatures, Am. Soc. for Testing Mat., STP No. 128 (1953), 184-221.

48. Grant, N. J., and Chaudhuri, A. R., "Creep and Fracture," in Creep and Recovery, Am. Soc. Metals, Cleveland, 1957, pp. 284-343.